Journal of Petrology Advance Access published September 21, 2006

The Somuncura Large Igneous Province in Patagonia: Interaction of a Transient Mantle Thermal Anomaly with a Subducting Slab

S. MAHLBURG KAY[1]*, A. A. ARDOLINO[2], M. L. GORRING[3] AND V. A. RAMOS[4]

[1]EARTH AND ATMOSPHERIC SCIENCES, SNEE HALL, CORNELL UNIVERSITY, ITHACA, NY 14853, USA

[2]DIRECCIÓN NACIONAL DE MINERÍA AND GEOLOGÍA, BUENOS AIRES, ARGENTINA

[3]EARTH AND ENVIRONMENTAL STUDIES, MONTCLAIR STATE UNIVERSITY, UPPER MONTCLAIR, NJ 07043, USA

[4]CIENCIAS EXACTAS AND NATURALES, CIUDAD UNIVERSITARIA, PABELLÓN II, 1428 BUENOS AIRES, ARGENTINA

RECEIVED JUNE 13, 2005; ACCEPTED AUGUST 23, 2006

The Oligo-Miocene Somuncura province is the largest (~55 000 km^2) back-arc mafic volcanic field in Patagonia, and one of Earth's largest with no clear link to a hotspot or major extension. Major and trace element and Sr–Nd–Pb isotopic data suggest involvement of a plume-like component in the mantle magma source mixed with hydrous, but not high field strength element (HFSE)-depleted components, from a disintegrating subducting plate. Magmatism is attributed to mantle upwelling related to disturbances during plate reorganization, possibly at a time when the South America plate was nearly stationary over the underlying mantle. Melting was enhanced by hydration of the mantle during Paleogene subduction. Crustal contamination was minimal in a refractory crust that had been extensively melted in the Jurassic. Eruption began with low-volume intraplate alkaline mafic flows with depleted Nd–Sr isotopic signatures. These were followed by voluminous ~29–25 Ma tholeiitic mafic flows with flat light and steep heavy rare earth element (REE) patterns, intraplate-like La/Ta ratios, arc-like Ba/La ratios and enriched Sr–Nd isotopic signatures. Their source can be explained by mixing EM1–Tristan da Cunha-like and depleted mantle components with subduction-related components. Post-plateau ~24–17 Ma alkaline flows with steep REE patterns, high incompatible element abundances, and depleted Sr–Nd isotopic signatures mark the ebbing of the mantle upwelling.

KEY WORDS: *Somuncura plateau; slab interaction; Patagonia; large igneous province (LIP); plume-like upwelling*

INTRODUCTION

Large basaltic provinces are commonly attributed to the activity of mantle plumes, recognized by associated regional thermal uplift and the time-transgressive tracks of the volcanic centers (e.g. Coffin & Eldholm, 1994). Numerous papers have focused on large igneous provinces (LIPs) such as Hawaii, the Paraná continental flood basalt province in South America, and continental rift volcanic fields such as those in Ethiopia. Less discussed have been intermediate-size volcanic provinces whose origins are not easily related to intracontinental rifting, mantle hotspots or extensive back-arc rifting. The purpose of this paper is to examine the geochemistry of one of the more enigmatic of these provinces, the Somuncura province of northern Patagonia (40·5° to 43°S; Figs 1 and 2). This province consists of a series of Oligocene to early Miocene volcanic fields that cover more than 55 000 km^2 in the Meseta de Somuncura and surrounding region.

Regionally, the Somuncura province is the largest of the post-Eocene mafic volcanic fields east of the Andean arc in Patagonia (Fig. 1) and the most difficult to explain in a geodynamic context. Further to the south, the extensive Miocene to Holocene plateau volcanic fields east of the Chile Triple Junction near 46·5° to 49·5°S have been explained in terms of mantle melting related to the opening of

*Corresponding author. Telephone: 1-607-255-4701. E-mail: smk16@cornell.edu

© The Author 2006. Published by Oxford University Press. All rights reserved. For Permissions, please e-mail: journals.permissions@oxfordjournals.org

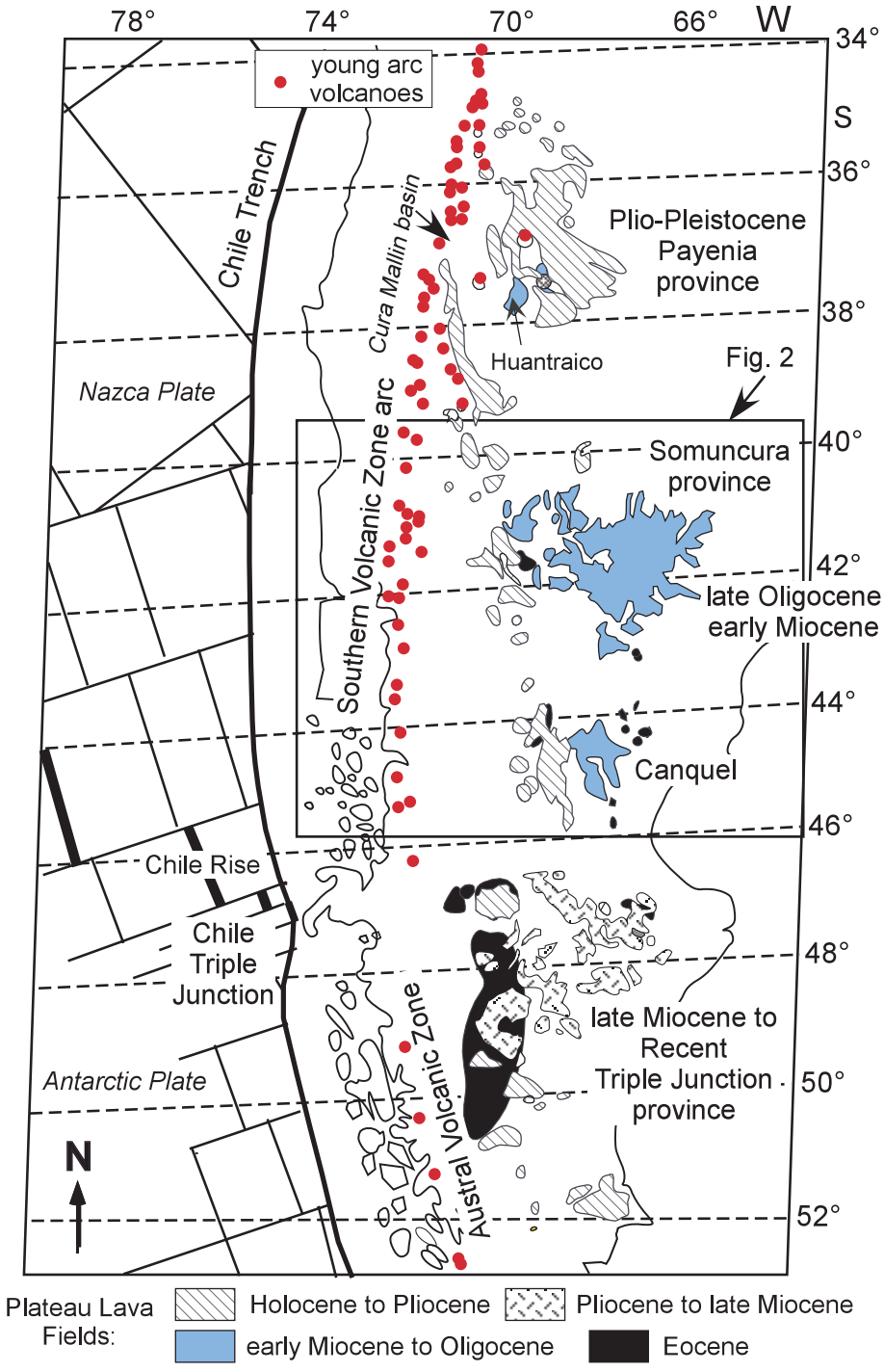

Fig. 1. Map of Patagonia and offshore region showing the location of the major Eocene to Holocene Patagonian back-arc plateau lava fields relative to the Chile trench, Nazca and Antarctic plates, Chile Triple Junction, and Holocene Southern Volcanic Zone and Austral Volcanic Zone arc centers (•). Rectangular area shows the location of Fig. 2.

an asthenospheric slab window in the subducting plate after collision of the Chile ridge with the Chile trench (Ramos & Kay, 1992; Gorring *et al.*, 1997; Gorring & Kay, 2001). To the north, the extensive Pliocene to Holocene 'Payenia' volcanic province east of the active Southern Volcanic Zone arc at 35° to 38°S has been related to melting of a hydrated mantle wedge above a steepening subduction zone

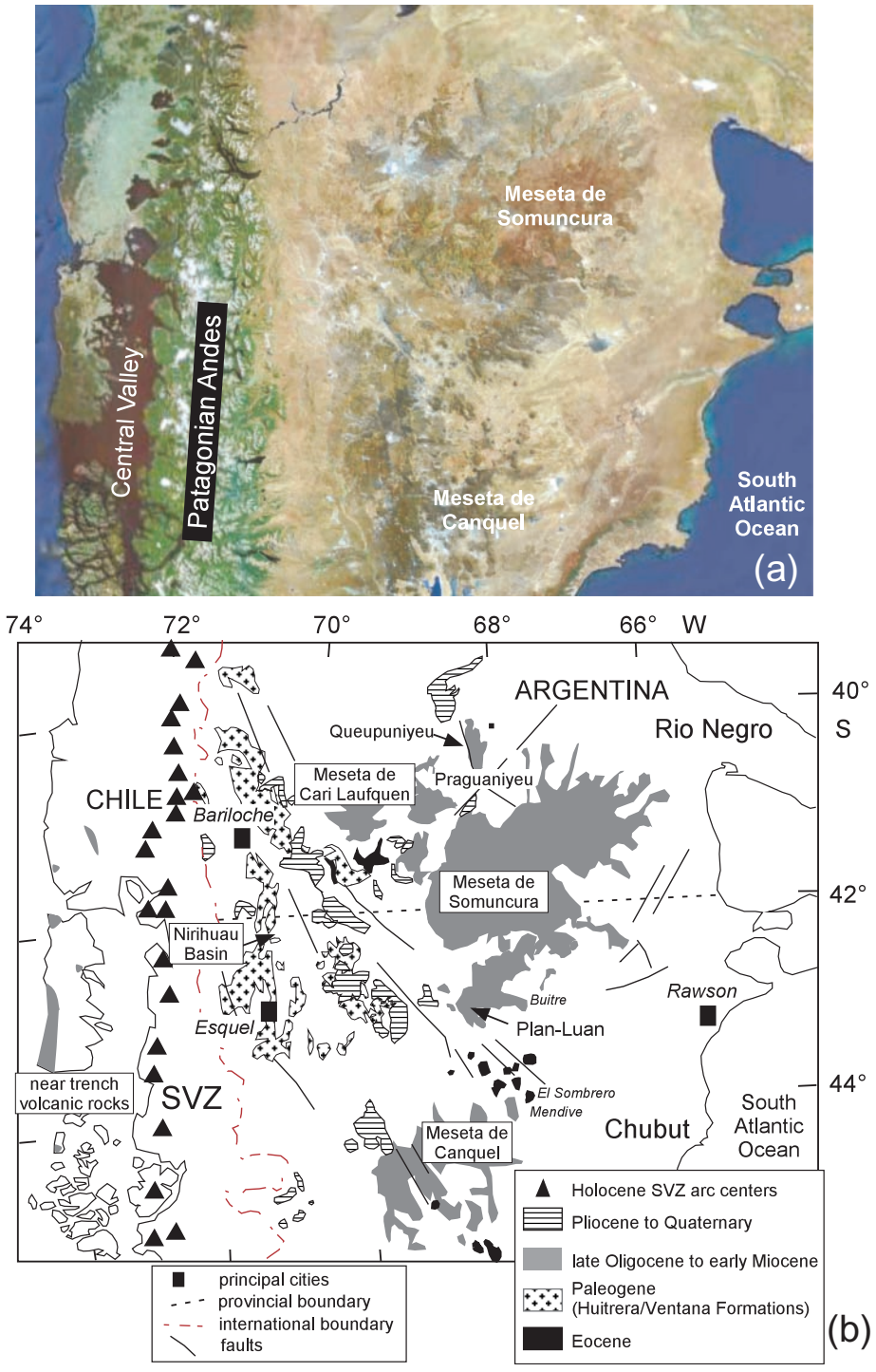

Fig. 2. (a) Thematic Mapper image of the region covered by the map in (b), showing the Meseta de Somuncura and Meseta de Canquel relative to the Patagonian Andes and the South Atlantic Ocean. The image is 850 km from west to east and was downloaded from Google Earth (earth.google.com). (b) Map of central Patagonia showing the location of the late Oligocene to early Miocene Somuncura volcanic province relative to Eocene back-arc volcanic rocks, the Paleogene arc and back-arc volcanic rocks of the Huitrera and Ventana Formations, Oligocene to early Miocene volcanic rocks in Chile, Pliocene to Quaternary back-arc volcanic rocks, and Holocene Southern Volcanic Zone (SVZ) arc centers (▲). Early Miocene high-K volcanic rocks and lower crustal xenoliths occur in the Plan-Luan region, high-Na volcanic rocks occur in the Queupuniyeu region, and mantle xenoliths occur in late Oligocene flows in the Praguaniyeu region. The Nirihuau basin is composed of Miocene volcaniclastic and sedimentary rocks. The figure is based on maps by Rapela & Kay (1988), Stern *et al.* (1990), Ardolino & Franchi (1993), Muñoz *et al.* (2000) and the 1:2 500 000 scale geological map of Argentina (1997, Servicio Geológico Minero Argentino, Buenos Aires).

(Kay, 2001; Kay *et al.*, 2004, 2006). The Somuncura province resembles these provinces in that there is little evidence for extension in the back-arc at the time of the eruptions (e.g. Kay *et al.*, 1993; Ardolino *et al.*, 1999). The only obvious contemporaneous tectonic association is that the Somuncura province eruptions preceded and coincided with the breakup of the Farallón plate, which caused a major change from oblique to near-normal convergence along the Andean margin (e.g. Cande & Leslie, 1986; Somoza, 1998). Kay *et al.* (1992, 1993) suggested that the Somuncura province was associated with a transient mantle thermal anomaly at the time of plate reorganization; de Ignacio *et al.* (2001) speculated that the thermal anomaly was due to a shallow asthenospheric upwelling caused by a concave-up slab geometry; and Muñoz *et al.* (2000) argued for an association with an asthenospheric slab window.

Within this geotectonic framework, the pre-plateau, plateau and post-plateau volcanic sequences of the Somuncura province are described. Major and trace element chemistry for 120 samples, $^{143}Nd/^{144}Nd$ and $^{87}Sr/^{86}Sr$ ratios for 34 samples, Pb isotopic analyses for 14 samples, and total-fusion $^{40}Ar/^{39}Ar$ ages for four samples are presented. These data are used to constrain the mantle and crustal sources and the tectonic setting of the Somuncura province magmas. The argument is made that the mantle signatures are little overprinted by crustal ones in accord with eruption through a crust whose low-temperature melting fraction was largely depleted in a Jurassic melting event (Kay *et al.*, 1989; Pankhurst & Rapela, 1995). A change from intraplate-like chemical signatures in the low-volume pre-plateau lavas to arc-like fluid-mobile element signatures in the voluminous plateau lavas is argued to reflect incorporation of subducted components into the mantle source as the plateau magmas formed. Tectonically, the Somuncura province is linked to a regionally hot mantle, preconditioned to melt by hydration related to Tertiary subduction. Melting is argued to be provoked by mantle instabilities related to plate reorganization, and possibly to a near-stationary position of the South American plate over the underlying mantle.

REGIONAL SETTING AND GENERAL DISTRIBUTION OF THE SOMUNCURA PROVINCE VOLCANIC ROCKS

The late Oligocene to Miocene volcanic rocks of the Somuncura province (Figs 2 and 3) overlie a late Precambrian to Paleozoic magmatic and metamorphic basement that is covered by the extensive Jurassic silicic volcanic rocks of the Chon Aike province (e.g. Kay *et al.*, 1989; Pankhurst & Rapela, 1995) as well as Cretaceous to Tertiary volcanic and sedimentary rocks (e.g. Rapela & Kay, 1988; Rapela *et al.*, 1988; Ardolino *et al.*, 1999). The location of the Somuncura province lavas relative to other Eocene to Miocene volcanic fields in the region is shown in Fig. 2b and the regional stratigraphy is shown in Table 1. Units shown in Fig. 2b include: (1) the Eocene to early Oligocene back-arc alkaline rocks in Argentina generally included in the El Buitre Formation (see Coira *et al.*, 1985; Lema & Cortés, 1987; Ardolino & Franchi, 1993; Ardolino *et al.*, 1999); (2) the arc and near back-arc volcanic rocks of the Eocene Huitrera and late Oligocene to early Miocene Ventana Formations to the west (e.g. Rapela *et al.*, 1988); and (3) the late Oligocene to middle Miocene arc and fore-arc rocks in Chile (Muñoz *et al.*, 2000).

The Somuncura province volcanic rocks consist of mafic lava flows and smaller volumes of silicic volcanic rocks, associated with large shield volcanoes. The most important centers seen on Thematic Mapper satellite images (Fig. 2a) are associated with silicic volcanic rocks in the Alta Sierra de Somuncura, and the Sierras of Telsen, Chacays, Apas and Talagapa (Fig. 3; see also Corbella, 1984; Remesal, 1988). Other possible centers are near Maquinchao and in the Meseta de Carri Laufquen region. Coalesced mafic flows from centers in the central and eastern parts of the region largely cover and surround the Meseta de Somuncura. This largely undissected plateau stands 200–700 m above the regional base level and has peaks rising to over 2000 m in the Alta Sierra de Somuncura. Some of the mafic flows from the Alta Sierra de Somuncura area reach the La Angostura, Ramos Mexía, and Aguada Cecilio regions, over 120 km to the north and east (Fig. 3). Observed flow sequence thicknesses range from several meters on the outer edge of the plateau to over 110 m in the Ranquil Huao valley (Fig. 3). Total thicknesses beneath the central Somuncura plateau are unknown. An indication of the initial area covered by the flows comes from remnants that cover more than 50 000 km^2 in the Meseta de Somuncura and $\sim$6600 km^2 in the Mesetas de Carri Laufquen, Coli Toro, and surrounding region (Fig. 3). For comparison, the flow remnants cover about a third of the estimated pre-erosional area (164 000 $\pm$ 5000 km^2) of the Columbia River province in North America, the total volume of which is estimated at 174 000 $\pm$ 31 000 km^3 (Tolan *et al.*, 1989).

Subdivisions of Somuncura province volcanic rocks on existing regional geological maps are inconsistent as they have traditionally been mapped using rock types, stratigraphic criteria and K/Ar ages rather than in

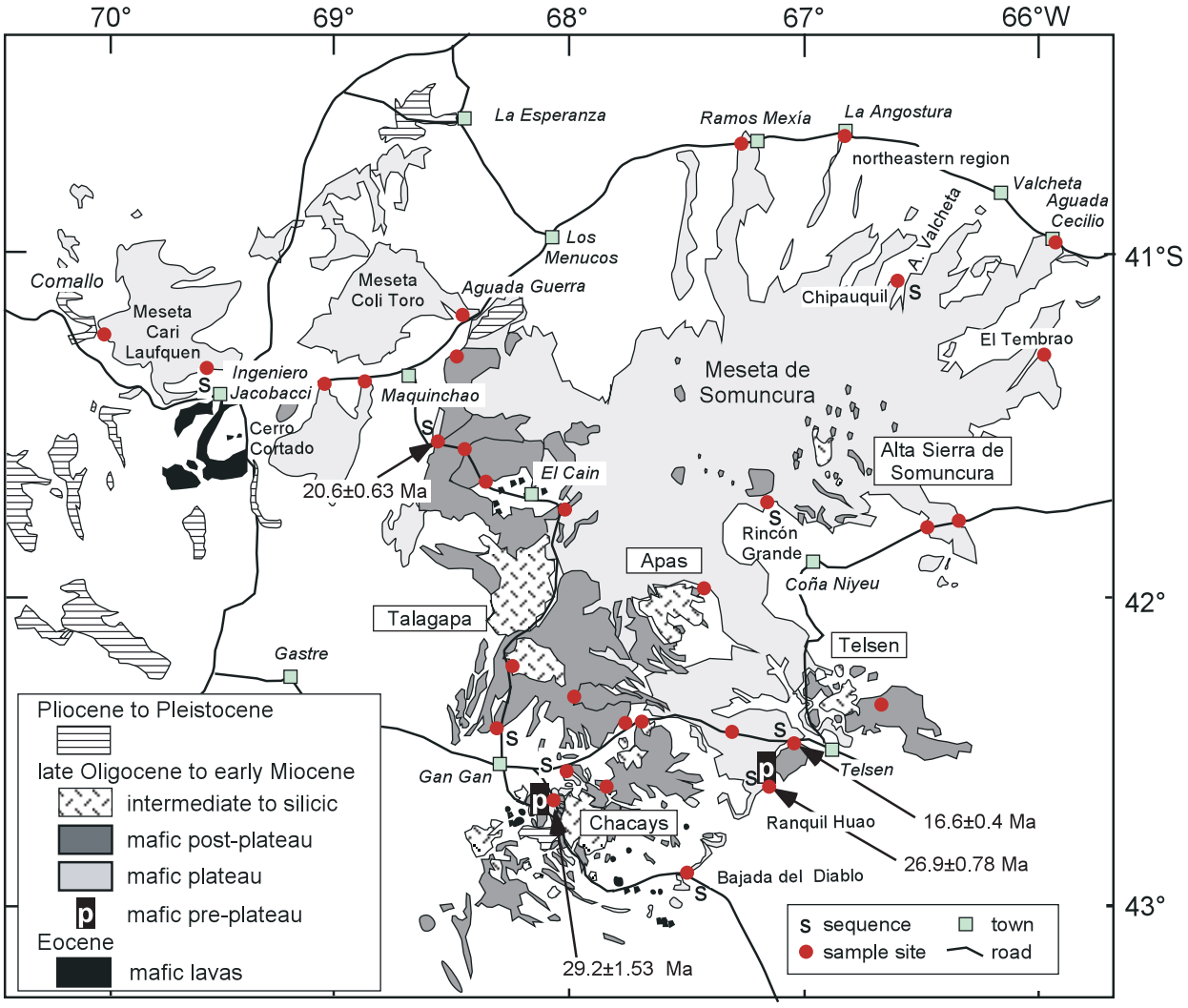

Fig. 3. Map of the late Oligocene to early Miocene Somuncura volcanic province showing the general distribution of mafic pre-plateau (marked **p**), plateau and post-plateau flows and intermediate to silicic volcanic rocks. Local formation names and stratigraphic details are given in Table 1. Principal eruptive centers are considered to be in the Alta Sierra de Somuncura, Apas-Chacays, Telsen, Talagapa and Carri Laufquen (Corbella, 1984; Coira *et al.*, 1985; Remesal, 1988). Also shown are Eocene and Pliocene to Pleistocene mafic volcanic rocks, new $^{40}Ar/^{39}Ar$ ages from Table 2, sample localities (●; S indicates a flow sequence), principal roads and place names used in the text (□, population centers). Map is based on Coira *et al.* (1985), Ardolino & Franchi (1993) and Servicio Geológico Minero Argentino (SERNAMIN) geological maps of the provinces of Rio Negro and Chubut.

relation to eruptive centers (see Ardolino & Franchi, 1993; Ardolino *et al.*, 1999; Remesal *et al.* 2002). The volcanic classification scheme used below and on the maps in Fig. 3 is shown in Table 1 relative to the regional formation names used by Ardolino *et al.* (1999). Roman numerals have been added to formation names when necessary to clarify age differences. The major volcanic divisions shown on the map in Fig. 3 are: (1) small-volume Eocene back-arc mafic lavas (El Buitre Formation); (2) small-volume mafic pre-plateau and voluminous plateau flows (respectively Somún Curá Formations I and II) that regionally overlie Sarmiento Formation I silicic tuffs that are not shown in Fig. 3; (3) mafic post-plateau flows (Quiñelaf Formation); (4) intermediate to silicic volcanic sequences (Sarmiento II, Quiñelaf Formations I and II). In the discussion below, the plateau units are locally subdivided into early, main and late divisions. Neither these divisions nor the pre-plateau flows are shown in Fig. 3 as they are not well differentiated across the entire region. Other Miocene volcanic rocks whose general localities are shown on Fig. 2b are the nephelinite, basinite, tephrite and phonolite flows described by Corbella (1984, 1989*a*, 1989*b*).

Table 1: *Stratigraphic framework*

Age	Terminology in this paper	Local formation names: mafic volcanic units	Local formation names: intermediate to silicic volcanic units	Formations in arc region in Argentina
Early to middle Miocene	post-plateau	Quiñelaf	Quiñelaf II*	Nirihuau (fluvial/lacustrine sediments)
Early Miocene to late Oligocene	late plateau	Somún Curá II*	Quiñelaf I*	Ventana (volcaniclastic sediments & lavas, shallow marine sediments)
	main plateau		Sarmiento II* (tuffs)	
	early plateau			
Oligocene	pre-plateau	Somún Curá I*	Sarmiento I* (tuffs)	Ventana (primarily andesitic lavas)
Eocene		El Buítre		Huitrera (mostly rhyolitic & volcanoclastic rocks)

*Roman number added for clarity (see text).

Table 2: *$^{40}Ar/^{39}Ar$ total-fusion ages of Somuncura province lavas*

Sample	Unit and location	K_2O (wt %)	^{39}Ar	% ^{40}Ar	Age (Ma ± 1σ)	Latitude	Longitude
CH1	Pre-plateau; Sierra de Chacays, near km 979, Route 11, south of Gan Gan	1·13	0·029	14·0	29·2 ± 1·53	42°38′S	68°10′W
RH3	Plateau; near top of Ranquil Huao sequence	0·78	0·068	19·5	26·9 ± 0·78	42°36′S	67°12′W
M2A	Post-plateau; top flow at Estancia El Triángulo, north of Route 5, south of Maquinchao	1·82	0·082	16·3	20·6 ± 0·63	41°29′S	68°36′W
TM1	Post-plateau; top flow, south of Route 4, west of village of Telsen	1·90	0·045	28·6	16·6 ± 0·4	42°28′S	67°00′W

Analytical methods discussed in text and by Gorring *et al*. (1997).

PHYSICAL CHARACTERISTICS, CHEMISTRY AND AGES OF THE SOMUNCURA PROVINCE VOLCANIC ROCKS

The descriptions of the physical characteristics, ages, petrology and geochemistry of the Somuncura pre-plateau, plateau and post-plateau volcanic groups below are based on published information, new field data, new $^{40}Ar/^{39}Ar$ ages in Table 2, the summary of K/Ar ages given by Ardolino & Franchi (1993), new major and trace element data in Tables 3–6 and Electronic Appendix Tables 1–5 that can be downloaded from http://petrology.oxfordjournals.org/, and new Sr, Nd and Pb isotopic data in Table 7. The data are plotted in Figs 4–12. The new analyses are for samples from across the region with an emphasis on sequences from the Ranquil Huao–Telsen region, the Rincón Grande and Coña Niyeu areas, the Chipauquil area south of Valcheta, north and east of Gan Gan, south and east of Maquinchao, the south–central Meseta Carri Laufquen, and south of the village of Comallo (Fig. 3). Sample locations are indicated in Fig. 3 and described in Table A1.

Analytical methods

Major element analyses were performed on a JEOL-733 Superprobe electron microprobe on glasses made from whole-rock powders in the facilities of the Materials Science Center at Cornell University. Samples were ground in a shatter-box in alumina containers. Silicic glasses contain a $Li_2B_4O_7$ flux. Analyses are averages of 4–6 spots in wavelength-dispersive mode with a 15 kV accelerating voltage, 15 nA beam current, 40 s count time, and a 30 μm beam diameter. Typical 2σ precision is ±1–5% relative at >1 wt %.

Trace elements were analyzed by instrumental neutron activation analysis (INAA) using the techniques

Table 3: *Whole-rock chemical compositions of Oligocene Somuncura pre-plateau lavas*

Region:	Chacays		Ranquil Huao					
Sample:	CH1	CH2A	RHA2	RHA1	RHB	RHC	RHD	RHE
Major and minor elements (wt %)								
SiO_2	48·73	49·28	45·18	49·54	48·78	49·54	51·14	50·45
TiO_2	2·30	1·93	2·69	1·71	2·37	1·48	2·04	1·99
Al_2O_3	16·18	16·64	15·22	15·47	16·46	16·96	17·48	17·08
FeO	10·32	11·52	10·61	11·08	10·79	11·85	10·31	9·95
MnO	0·17	0·15	0·19	0·15	0·19	0·15	0·16	0·18
MgO	8·08	6·92	9·04	7·08	6·04	5·08	4·07	4·47
CaO	8·47	7·99	9·83	8·34	7·90	8·90	6·89	6·86
Na_2O	3·27	3·60	3·40	4·50	4·79	3·78	4·64	4·80
K_2O	1·13	1·05	2·46	1·79	1·93	0·98	1·55	2·48
P_2O_5	0·67	0·65	1·25	0·63	—	0·30	1·09	—
Total	99·32	99·73	99·87	100·29	99·25	99·02	99·37	98·26
Trace elements (ppm)								
La	28·3	28·6	66·5	44·5	73·6	19·1	62·6	73·1
Ce	56·4	58·4	132·6	85·8	145·5	40·3	128·4	140·9
Nd	27·2	28·7	57·2	37·3	57·3	19·0	53·4	53·2
Sm	6·08	6·44	9·96	6·77	9·72	4·60	9·07	9·05
Eu	1·98	2·07	2·83	1·93	2·74	1·41	2·39	2·49
Tb	0·816	0·909	1·18	0·862	1·08	0·760	0·998	1·00
Yb	1·58	1·97	2·32	1·85	2·20	2·05	2·49	2·17
Lu	0·207	0·252	0·285	0·246	0·295	0·267	0·350	0·328
Sr	681	604	1224	763	1100	504	987	1077
Ba	472	477	673	486	935	289	853	861
Cs	0·25	0·36	0·43	0·83	0·68	0·15	1·69	0·76
U	0·8	0·6	2·4	1·5	2·1	0·4	2·2	1·5
Th	2·9	2·4	6·3	5·5	8·7	2·2	7·5	8·7
Hf	3·7	3·8	7·1	6·1	9·0	3·4	8·8	9·7
Ta	2·5	2·2	6·3	3·7	6·4	1·5	5·7	6·5
Sc	18·8	21·8	24·2	18·3	14·0	22·6	15·4	11·3
Cr	257	162	266	223	130	254	148	84
Ni	168	89	140	176	71	179	110	51
Co	45	45	45	48	35	58	31	28

Major elements by electron microprobe on fused glasses; trace elements by INAA. (See discussion of analytical details in text.) Blank elements were not measured. LOI (loss on ignition) not determined. Sample locations are given in Table A1.

and standards discussed by Kay *et al.* (1987). Powders were packed in ultrapure Suprasil® quartz tubes, irradiated in a TRIGA reactor in Ward Laboratory at Cornell University at a power level of ~400 kW for 3–4 h, and counted for 4–10 h after 6 and ~40 days, respectively, on an Ortec intrinsic Ge detector. Precision (2σ) based on multiple analyses of Cornell internal standard PAL is ±2% for all elements except U, Sr, Nd, and Ni, which have precisions of ±8–12%. Y, Rb, Sr and Zr concentrations in samples GG2, GG5 and M12 were determined by X-ray fluorescence (XRF) analysis at the Universidad Nacional de Jujuy in Argentina using US Geological Survey (USGS) standards.

Isotopic ratios were measured on a multi-collector VG Sector 54 thermal ionization mass spectrometer in the Keck Geochemistry Laboratory at Cornell University using the chemical and analytical techniques described by White & Duncan (1996). Average standard values for over 50 measurements of NBS987 give $^{87}Sr/^{86}Sr = 0{\cdot}710235 \pm 34$ (2σ); La Jolla $^{143}Nd/^{144}Nd = 0{\cdot}511864 \pm 14$ (2σ); and NBS981 $^{206}Pb/^{204}Pb = 16{\cdot}895 \pm 20$, $^{207}Pb/^{204}Pb = 15{\cdot}438 \pm 20$ and

Table 4: Whole-rock chemical compositions of late Oligocene to early Miocene Somuncura plateau lavas

Region:	Ranquil Huao						Telsen	Gan Gan				Coña Niyeu		Coña Niyeu sequence				
Sample:	RHF	RHG	RH5	RH4	RH2	RH1	TM2	GG7D	GG8	GG9E	GG9C	CN1	CN3	CN4AA	CN4B	CN4C	CN4D′	CN4F
Major and minor elements (wt %)																		
SiO_2	49·85	49·73	49·44	50·03	50·93	50·53	51·80	49·64	52·95	52·59	52·59	51·66	54·45	53·60	51·26	50·92	53·70	53·36
TiO_2	1·37	1·82	1·85	2·01	1·79	1·71	1·58	1·87	1·64	1·97	1·52	1·49	1·40	1·94	2·02	1·59	1·63	1·76
Al_2O_3	16·86	15·95	15·96	15·91	15·94	16·20	15·63	15·01	16·26	16·59	16·42	16·48	16·04	15·37	15·05	14·63	14·91	15·15
FeO	11·97	12·12	12·07	11·43	11·25	11·29	10·51	10·16	9·00	9·74	9·90	10·65	9·84	9·52	11·24	11·30	10·18	9·76
MnO	0·19	0·14	0·15	0·15	0·12	0·17	0·15	0·15	0·13	0·13	0·12	0·14	0·12	0·14	0·14	0·18	0·10	0·14
MgO	5·11	6·43	6·63	7·18	7·04	6·43	6·41	8·24	5·34	4·53	5·48	5·87	6·41	6·31	7·76	8·52	6·13	5·52
CaO	9·47	8·87	8·49	8·28	8·03	8·19	8·72	10·06	8·56	8·37	8·83	8·85	7·26	8·10	8·47	8·53	7·93	8·46
Na_2O	3·60	3·62	3·75	3·77	3·63	3·78	3·37	3·27	3·30	3·22	3·52	3·82	3·74	3·79	3·53	3·27	3·61	3·53
K_2O	0·61	0·78	0·76	0·79	0·66	0·68	0·69	1·06	1·51	0·94	1·03	0·79	0·40	1·08	0·57	0·40	0·74	1·10
P_2O_5	0·21	0·39	0·36	0·39	0·32	—	0·30	0·35	0·36	0·48	0·32	—	0·21	—	—	0·23	0·34	0·37
Total	99·24	99·85	99·46	99·94	99·71	98·98	99·16	99·81	99·05	98·56	99·73	99·75	99·87	99·85	100·04	99·57	99·27	99·15
Trace elements (ppm)																		
La	15·9	13·1	13·2	17·5	13·1	13·8	13·2	16·2	19·5	18·7	18·9	14·0	8·88	19·3	11·2	9·37	14·2	15·0
Ce	32·0	27·1	26·7	38·7	29·3	30·4	29·2	33·2	38·8	36·9	32·9	28·3	18·0	38·6	23·4	20·0	28·7	32·5
Nd	15·0	13·9	12·4	15·7	15·4	18·4	14·0	18·2	19·6	18·7	21·4	15·0	11·5	20·9	15·0	12·7	18·1	19·5
Sm	3·83	3·70	3·47	5·15	4·40	4·44	4·09	4·53	4·59	4·89	5·02	3·76	3·49	5·12	4·17	3·51	4·79	5·31
Eu	1·31	1·25	1·22	1·62	1·48	1·46	1·41	1·49	1·48	1·60	1·64	1·19	1·19	1·60	1·35	1·25	1·57	1·67
Tb	0·679	0·707	0·669	0·776	0·708	0·729	0·742	0·706	0·773	0·784	0·851	0·639	0·636	0·746	0·655	0·614	0·720	0·775
Yb	1·82	1·82	1·77	1·54	1·66	1·58	1·51	1·56	1·56	1·78	2·07	1·61	1·41	1·65	1·50	1·41	1·59	1·52
Lu	0·254	0·244	0·244	0·235	0·214	0·203	0·219	0·200	0·213	0·238	0·313	0·207	0·188	0·210	0·205	0·177	0·197	0·217
Sr	383	455	384	548	457	554	543	504	549	567	529	477	421	639	673	512	796	980
Ba	168	188	216	239	196	247	267	324	324	361	348	243	180	447	242	208	422	571
Cs	0·03	0·09	1·08	0·11	0·07	0·13	0·11	0·16	0·18	0·23	0·27	0·37	0·14	0·36	0·24	0·16	0·17	0·27
U	0·32	0·49	0·39	0·44	0·32	0·31	0·4	0·4	0·5	1·6	0·7	0·6	0·3	0·7	0·3	0·3	0·3	0·3
Th	1·6	1·5	1·4	1·7	1·5	1·5	1·5	1·7	2·0	2·7	2·5	2·0	1·3	2·7	1·0	0·9	1·2	1·2
Hf	2·4	2·3	2·3	3·2	2·7	2·7	2·6	3·0	3·0	3·7	2·9	2·1	1·9	3·2	2·2	1·9	2·3	2·4
Ta	1·2	1·0	1·0	1·6	1·1	1·1	1·1	1·4	1·7	1·6	1·3	0·97	0·68	1·50	0·80	0·90	0·80	0·80
Sc	22·1	24·2	22·8	21·2	20·4	19·8	19·7	19·9	17·7	19·2	22·4	18·2	17·8	17·3	20·8	21·1	19·1	18·1
Cr	243	179	194	284	260	272	294	298	281	342	381	184	255	242	336	338	292	243
Ni	168	116	131	213	196	202	217	182	188	110	143	115	170	162	197	228	182	134
Co	53	48	50	53	51	51	57	47	42	37	40	47	44	40	50	61	42	41

Region:	Aguada Cecilio		Valcheta				La Angostura	Mexía	Coli Toro	Maquinchao			Cari Laufquen		Comallo	
Sample:	B26	B19	Val3-1	Val3-2	Val3-4	Val3-5	Ang1A	B31	Som4	M1	Mac3B	Pat12B	Pat11A	Pat11B	Pat15A	Pat15C
Major and minor elements (wt %)																
SiO_2	53·69	52·95	52·85	52·50	52·16	51·98	—	54·16	51·85	49·13	49·17	49·74	53·72	53·26	52·85	53·67
TiO_2	1·52	1·43	1·61	1·71	1·59	1·76	—	1·38	1·54	1·56	1·93	1·74	2·23	2·29	1·28	1·25
Al_2O_3	15·45	15·34	15·71	14·82	14·75	16·27	—	15·59	15·28	16·34	16·57	16·89	16·01	15·84	16·04	16·09
FeO	10·44	9·95	10·05	10·38	10·11	9·79	11·42	10·07	10·89	10·58	10·47	10·06	9·38	9·63	10·15	9·74
MnO	0·14	0·15	0·15	0·15	0·16	0·12	—	0·11	0·12	0·18	0·19	0·08	0·08	0·16	0·23	0·21
MgO	5·40	7·30	7·31	7·55	7·66	5·75	—	5·87	6·09	7·46	5·52	5·23	5·48	6·07	7·29	7·19
CaO	8·11	8·49	7·34	7·77	8·11	8·64	—	8·60	8·88	9·22	9·23	11·27	7·98	7·35	8·12	7·87
Na_2O	3·75	3·41	3·59	3·62	3·53	3·70	4·16	3·80	3·10	3·46	3·93	3·72	3·99	4·24	3·48	3·65
K_2O	0·42	0·52	0·90	0·85	0·84	0·76	—	0·29	0·70	0·94	1·17	0·84	0·85	1·44	0·49	0·44

Table 4: continued

Region:	Aguada Cecilio		Valcheta				La Angostura	Mexía	Coli Toro	Maquinchao			Cari Laufquen		Comallo	
Sample:	B26	B19	Val3-1	Val3-2	Val3-4	Val3-5	Ang1A	B31	Som4	M1	Mac3B	Pat12B	Pat11A	Pat11B	Pat15A	Pat15C
P_2O_5	–	–	–	–	–	–	–	–	–	0·30	0·47	–	–	–	–	–
Total	98·92	99·54	99·51	99·35	98·91	98·77	–	99·87	98·45	99·17	98·65	99·57	99·72	100·28	99·93	100·11
Trace elements (ppm)																
La	6·60	10·3	16·7	16·6	16·0	16·5	6·88	7·61	12·2	18·0	26·3	18·8	14·1	24·6	5·83	6·15
Ce	16·8	23·0	35·8	35·4	35·1	33·6	19·5	18·2	25·8	36·7	51·9	39·2	32·7	56·0	14·7	15·6
Nd	12·0	15·0	21·1	20·0	17·7	19·7	11·2	13·4	14·9	16·0	27·3	20·1	19·0	34·8	10·7	10·1
Sm	3·71	3·61	4·86	4·70	4·57	5·06	3·71	3·68	4·22	4·55	5·46	4·77	5·53	7·91	3·64	3·66
Eu	1·29	1·28	1·49	1·44	1·42	1·66	1·40	1·29	1·39	1·36	1·76	1·45	1·80	2·31	1·17	1·20
Tb	0·636	0·587	0·752	0·700	0·704	0·754	0·745	0·659	0·713	0·704	0·826	0·698	0·789	1·17	0·703	0·730
Yb	1·45	1·34	1·59	1·72	1·57	1·56	1·56	1·52	1·70	2·13	1·80	1·48	1·67	2·37	1·76	1·78
Lu	0·188	0·164	0·215	0·231	0·211	0·195	0·213	0·194	0·226	0·262	0·233	0·203	0·224	0·324	0·243	0·236
Sr	414	553	502	508	504	692	483	451	455	535	895	618	622	688	384	400
Ba	154	415	335	316	309	353	153	182	253	273	438	437	299	515	168	186
Cs	0·48	0·27	0·42	0·50	0·53	0·16	0·14	0·06	0·26	0·34	0·19	0·09	0·22	0·41	0·28	0·29
U	0·3	0·4	0·54	0·94	0·85	0·40	0·32	0·20	0·35	0·6	0·56	0·43	0·30	0·71	0·11	0·18
Th	1·2	1·5	2·3	2·6	2·5	1·5	0·9	0·77	1·7	2·4	2·7	1·7	1·0	2·3	0·7	0·9
Hf	1·9	2·0	3·1	3·1	3·0	2·6	2·2	2·1	2·4	3·0	3·4	2·6	3·0	4·9	1·8	1·8
Ta	0·59	0·75	1·1	1·1	1·1	1·1	0·47	0·57	0·86	1·3	2·1	1·4	0·9	1·7	0·33	0·31
Sc	21·3	18·2	18·8	19·9	19·3	18·1	21·7	17·7	20·0	27·8	21·5	21·8	17·8	17·5	18·9	18·4
Cr	224	293	344	333	327	153	356	255	316	250	276	276	135	182	321	323
Ni	158	205	221	192	192	103	181	164	200	127	137	102	92	126	209	190
Co	49	48	48	48	47	42	49	47	44	47	44	39	38	40	46	43

Major elements by electron microprobe on fused glasses; trace elements by INAA. (See discussion of analytical details in text.) Blank elements were not measured. LOI not determined. Sample locations are given in Table A1.

$^{208}Pb/^{204}Pb = 36{\cdot}541 \pm 60$. Mass fractionation corrections assume $^{86}Sr/^{88}Sr = 0{\cdot}1194$, $^{146}Nd/^{144}Nd = 0{\cdot}7219$, $^{206}Pb/^{204}Pb = 16{\cdot}937$, $^{207}Pb/^{204}Pb = 15{\cdot}493$ and $^{208}Pb/^{204}Pb = 36{\cdot}705$. Total procedural blanks for Sr, Nd, and Pb are <150 pg. $^{87}Sr/^{88}Sr$ and $^{143}Nd/^{144}Nd$ ratios are age-corrected based on trace element data in Tables 3–6 with Rb concentrations being estimated from similar analyses by Remesal (1988), Corbella (1989*a*), Corbella & Barbieri (1989) and Remesal *et al.* (2002) where unavailable. Errors from Rb estimation are small as Sr/Rb ratios are all 25 or greater.

$^{40}Ar/^{39}Ar$ analyses were carried out by total fusion of bulk samples (10–350 mg, 250–350 μm size fraction) at Lehigh University on a VG3600 mass spectrometer operating in static mode at an accelerating voltage of 4·5 kV. Age uncertainties include an error in the J factor of <2%. All isotopic ratios are corrected for line blank contributions, mass discrimination, orifice corrections, and interfering reactions on K and Ca. Details of the analytical procedure have been given by Gorring *et al.* (1997).

Pre-plateau flows

On a regional scale, the pre-plateau flows erupted back-arc to a broad region of arc volcanic centers that were most active between ~32 and 29 Ma (Cazau *et al.*, 1987; Rapela *et al.*, 1988; Muñoz *et al.*, 2000). Volcanic rocks from these centers comprise the Ventana Formation in Argentina (see Rapela *et al.*, 1988) and also occur near the Chilean coast some 300 km to the west (Muñoz *et al.*, 2000). These centers erupted east of the subducting Farallón plate, which was converging at an angle of ~55–60° NE with the South America plate at a velocity of <5 cm/year (Somoza, 1998).

The pre-plateau flows are volumetrically minor, back-arc alkali basalts and hawaiites that erupted from small volcanic centers that are now largely obscured by erosion or a cover of younger flows. Their overall distribution is not well known. The two localities examined here are the basal flows in the Quebrada Ranquil Huao and the Sierra de Chacays (Fig. 3). The setting of the Ranquil Huao flows has been described by Remesal *et al.* (2002). Their absolute age is uncertain. The age of the basal

Table 5: *Whole-rock chemical compositions of early to middle Miocene Somuncura post-plateau lavas*

Region:	Bajada del Diablo		Chacays	Apas	Telsen		Bajo Hondo		Gan Gan			Maquinchao			
Sample:	CH4B	CH5A	Ard304	Ard101a	TM1	Ad209	Ard58	Ard68	GG7A	GG7B	GG9A	M2A	M2B	M2C	M5
Major and minor elements (wt %)															
SiO_2	50·77	50·94	50·01	48·44	52·90	53·04	49·64	49·73	50·99	50·26	51·92	48·27	48·79	48·77	47·94
TiO_2	1·85	2·14	2·01	2·17	2·70	2·88	3·28	2·93	2·42	2·65	2·22	3·01	3·09	3·17	2·82
Al_2O_3	15·94	15·94	16·08	16·39	15·17	15·02	16·32	16·47	16·34	15·44	16·30	17·30	16·98	17·30	16·89
FeO	10·74	10·57	10·12	11·16	9·91	10·65	10·38	9·86	9·75	9·99	9·12	11·26	11·82	11·32	11·38
MnO	0·14	0·12	0·09	0·13	0·11	0·06	0·17	0·17	0·13	0·12	0·15	0·22	0·17	0·22	0·16
MgO	4·57	6·21	6·54	5·95	5·10	4·82	4·81	5·17	5·32	5·38	3·94	4·62	4·17	3·70	3·67
CaO	8·84	7·36	7·78	9·63	7·34	7·14	9·60	8·63	7·89	8·20	7·52	8·69	7·31	8·35	8·61
Na_2O	3·82	4·51	3·58	3·66	4·01	3·86	3·39	3·58	4·05	4·14	3·87	3·99	4·43	3·98	4·11
K_2O	2·06	1·46	2·43	1·23	1·90	1·68	1·98	2·69	2·52	2·48	2·72	1·82	2·05	1·64	1·61
P_2O_5	0·57	0·63	—	—	0·59	—	—	—	0·70	0·68	0·78	0·72	0·73	0·57	0·71
Total	99·30	99·88	98·64	98·76	99·73	99·15	99·57	99·23	100·11	99·34	98·54	99·90	99·54	99·02	97·90
Trace elements (ppm)															
La	37·9	27·1	41·7	25·0	28·2	27·3	40·9	51·4	38·7	41·3	39·0	41·1	48·0	44·8	49·8
Ce	73·7	55·6	82·7	53·7	61·0	60·0	89·6	108·7	77·6	80·6	76·5	80·6	102·5	88·6	98·9
Nd	33·6	29·7	39·5	28·1	40·6	34·0	45·7	55·0	41·0	36·4	40·6	38·1	45·6	41·8	46·2
Sm	6·73	6·69	7·17	5·88	8·61	7·89	8·81	9·27	8·22	7·31	7·59	7·67	8·72	8·21	8·37
Eu	2·04	2·25	2·22	1·86	2·83	2·70	3·02	2·85	2·57	2·43	2·71	2·38	2·68	2·52	2·60
Tb	0·873	0·878	0·999	0·840	1·09	1·09	1·06	1·10	1·02	0·927	0·994	0·990	1·09	1·03	1·04
Yb	2·10	1·63	2·01	1·75	1·77	1·86	2·13	1·98	1·96	1·94	1·91	2·11	2·26	2·13	2·27
Lu	0·257	0·191	0·255	0·229	0·254	0·216	0·261	0·257	0·247	0·239	0·249	0·271	0·329	0·294	0·296
Sr	711	793	749	735	745	724	1054	1087	767	668	776	958	1054	942	927
Ba	647	582	680	427	818	687	1073	838	732	995	1012	944	1185	973	1216
Cs	0·29	0·23	0·35	0·18	0·17	0·14	0·20	0·24	0·38	0·22	0·19	0·39	0·58	0·43	1·23
U	1·22	1·02	1·13	0·29	0·50	0·46	0·98	1·28	1·05	1·28	1·34	1·12	0·88	1·04	1·65
Th	4·5	2·4	4·3	2·3	2·1	2·0	3·1	4·3	3·7	4·4	3·9	4·3	5·2	5·0	6·1
Hf	5·7	3·9	5·2	3·5	4·4	4·2	6·0	7·1	6·3	6·2	5·4	4·4	5·4	4·9	5·7
Ta	2·8	2·0	3·2	2·2	1·7	1·7	2·8	3·9	3·2	3·4	3·1	3·6	4·4	4·1	4·1
Sc	24·9	17·7	18·3	23·6	16·3	16·0	23·1	19·5	19·0	17·7	17·8	19·7	18·4	16·9	18·2
Cr	352	181	225	267	141	130	72	153	197	251	242	49	8	8	18
Ni	138	128	131	136	83	78	52	76	133	238	122	27	15	13	23
Co	51	41	40	50	38	33	39	37	39	44	36	38	36	34	37

Major elements by electron microprobe on fused glasses; trace elements by INAA. (See discussion of analytical details in text.) Blank elements were not measured. LOI not determined. Sample locations are given in Table A1. Additional analyses are given in Electronic Supplement Table 3.

Sierra de Chacays flow is constrained by a new $^{40}Ar/^{39}Ar$ total-fusion age of 29·2 ± 1·5 Ma in Table 2.

The pre-plateau flows are chemically distinct from the younger plateau and post-plateau flows. Those in the Ranquil Huao sequence are olivine–clinopyroxene-bearing basanites and olivine–clinopyroxene–plagioclase-bearing hawaiites (Remesal *et al.* 2002), whereas those in the Sierra de Chacays are olivine–pyroxene–plagioclase-bearing alkali olivine basalts (Table 3 and Fig. 4). The Ranquil Huao flows are notable among Somuncura province flows for their high light rare earth element (LREE) contents (Ce = 85–150) and steep REE patterns (La/Yb = 24–34, La/Sm = 6·6–8·2; Figs 5a and 6); low ratios of alkali, alkaline earth, and Th to REE and high field strength elements (HFSE) (e.g. Ba/La < 13; Ba/Ta < 150; La/Ta = 10·6–12·1,Th/Ta = 1–1·5, Th/La < 0·15; Figs 7 and 8); low $^{87}Sr/^{86}Sr$ ratios (0·7034); high εNd values

Table 6: Whole-rock chemical compositions of other Somuncura region volcanic rocks

Unit:	Late Oligocene to early Miocene Quiñelaf (I & II) Fm						Jurassic Chon Aike rhyolite		Oligocene arc region: ~31–28 Ma				
Region:	East of Gan Gan				Talagapa		Telsen		Ventana	west Maiten		Reyhuao	
Sample:	GG5	GG3	GG4	GG2	M13	M12	453	458	CV82	WM2	WM5	RE4	RE1
Major and minor elements (wt %)													
SiO_2	59·04	59·57	63·18	71·22	67·66	71·80	71·76	77·67	49·91	55·85	56·73	49·50	48·94
TiO_2	1·12	1·07	0·48	0·17	0·77	0·15	0·40	0·16	1·45	1·37	1·52	1·41	1·43
Al_2O_3	19·02	18·81	19·21	14·07	15·85	14·46	14·28	12·44	17·32	18·04	17·99	17·30	18·20
FeO	5·24	4·87	4·18	3·30	3·25	2·47	2·40	0·83	9·00	7·87	7·94	9·04	9·59
MnO	0·14	0·03	0·12	0·15	0·18	1·15	0·05	0·04	0·15	0·14	0·14	0·16	0·16
MgO	1·51	1·01	0·48	0·01	0·45	1·50	0·98	0·08	7·81	3·58	3·56	7·28	6·04
CaO	3·38	2·87	1·27	0·29	1·13	1·48	1·96	0·31	10·80	6·14	6·51	7·84	8·36
Na_2O	5·43	5·31	5·27	6·23	4·99	2·62	3·01	3·07	2·59	4·76	4·20	3·78	3·66
K_2O	4·58	5·57	5·48	4·57	5·52	4·43	5·05	5·37	0·45	0·83	0·85	0·80	0·78
P_2O_5	0·44	0·35	0·19	—	0·19	0·02	0·09	0·04	0·39	0·33	0·34	0·58	0·58
Total	99·90	99·46	99·86	100·01	99·99	100·07	99·98	100·01	99·87	98·91	99·78	97·69	97·74
Trace elements (ppm)													
La	46·8	53·8	56·0	168·4	88·4	103·8	52·2	16·1	8·1	11·0	11·0	16·1	15·9
Ce	84·6	96·8	103·1	288·6	179·4	230·2	103·8	42·8	19·0	29·8	28·5	39·4	37·0
Nd	36·0	42·7	44·2	105·8	70·3	80·2	37·3	18·3	13·1	16·1	19·1	24·3	26·0
Sm	6·25	7·57	7·56	18·8	12·0	15·4	6·3	6·06	3·42	5·35	4·97	6·17	5·91
Eu	2·18	2·27	1·71	0·328	1·20	0·33	1·09	0·103	1·18	1·66	1·52	1·77	1·64
Tb	0·738	0·899	0·910	2·12	1·27	2·24	0·652	1·37	0·649	1·038	0·928	1·112	1·118
Yb	1·93	3·10	2·52	6·58	3·87	6·77	1·88	7·97	2·24	3·37	3·07	2·92	2·93
Lu	0·288	0·499	0·377	0·827	0·511	0·810	0·242	1·05	0·303	0·483	0·451	0·432	0·439
Y	23	—	—	48	—	63	—	—	—	—	—	—	—
Rb	66	—	—	319	—	197	—	—	29	16	—	7	5
Sr	605	506	221	37	158	74	318	14	295	347	—	330	331
Ba	903	1139	598		452	23	759	22	156	198	136	175	148
Cs	0·73	0·75	0·83	3·3	1·6	3·4	4·8	27·3	0·98	0·31	0·50	0·06	0·25
U	1·9	2·2	2·2	7·9	5·1	6·0	2·1	3·7	0·38	0·25	0·16	0·43	0·33
Th	6·6	8·3	9·6	45·4	18·8	24·0	12·3	19·7	1·0	1·4	1·8	0·9	1·1
Zr	447	—	—	1388	—	853	—	—	—	—	—	—	—
Hf	8·5	9·4	5·3	33·8	15·6	22·0	5·5	3·3	2·2	4·5	4·2	4·3	4·4
Ta	4·0	5·1	5·4	20·9	6·1	9·8	1·4	—	0·51	0·48	0·40	0·42	0·38
Sc	7·1	6·5	4·8	0·8	4·9	2·8	4·6	5·2	34·3	17·6	19·6	24·6	25·0
Cr	11	2	1	0	1	3	4	<1	267	22	32	255	239
Ni	13	11	5	1	1	<1	4	<1	123	16	35	120	114
Co	9	5	3	0	2	1	5	<1	40	27	26	36	35

Major elements by electron microprobe on fused glasses; most trace elements by INAA; Y, Zr and Rb by XRF. (See discussion of analytical details in text.) Blank elements were not measured. Quiñelaf sample localities are given in Table A1. Major element, Rb and Sr analyses of Oligocene arc samples are from Rapela *et al.* (1988). Additional analyses are given in Electronic Supplement Table 4.

Table 7: Sr–Nd–Pb isotopic and whole-rock SiO_2 compositions of Somuncura province volcanic rocks

Sample	Region	SiO_2 (wt %)	$^{87}Sr/^{86}Sr$ measured	$^{87}Sr/^{86}Sr$ initial	$^{143}Nd/^{144}Nd$ measured	$^{143}Nd/^{144}Nd$ initial	εNd initial	$^{206}Pb/^{204}Pb$ measured	$^{207}Pb/^{204}Pb$ measured	$^{208}Pb/^{204}Pb$ measured
Pre-plateau flows				*at 29 Ma*		*at 29 Ma*				
RHA2	Ranqui Huao	44·7	0·703414	0·703385*	0·512855	0·512836	+4·6	18·733	15·632	38·626
RHB	Ranqui Huao	48·8	0·704033	0·704001*	0·512752	0·512734	+2·6	—	—	—
CH1	Chacays	48·7	0·704023	0·704004*	0·512736	0·512712	+2·1	18·584	15·611	38·474
Plateau flows				*at 27 Ma*		*at 27 Ma*				
RHG	Ranquil Huao	49·7	0·704308	0·704284*	0·512692	0·512664	+1·2	18·308	15·599	38·375
RH4	Ranquil Huao	50·0	0·704588	0·704545*	0·512692	0·512657	+1·1	—	—	—
RH2	Ranquil Huao	50·9	0·704689	0·704665*	0·512630	0·512600	−0·07	18·197	15·607	38·394
RH1	Ranquil Huao	50·5	0·704655	0·704635*	0·512670	0·512644	+0·80	—	—	—
GG9C	Gan Gan	52·6	0·704552	0·704508*	0·512647	0·512622	+0·37	—	—	—
CN3	Coña Niyeu	53·6	0·704631	0·704589*	—	—	—			
CN4A	Coña Niyeu	53·5	0·704255	0·704231*	0·512660	0·512635	+6·1	18·280	15·592	38·298
CN4AA	Coña Niyeu	53·6	0·704299	0·704273*	0·512617	0·512591	−0·24	—	—	—
CN4C	Coña Niyeu	50·9	0·704327	0·704303*	0·512675	0·512646	+0·82	—	—	—
CN4F	Coña Niyeu	53·4	0·704586	0·704552*	0·512580	0·512551	−1·02	—	—	—
B26	Aguada Cecilio	53·7	0·704447	0·704404*	0·512617	0·512584	−0·37	—	—	—
B19	Aguada Cecilio	53·0	0·704483	0·704451*	0·512603	0·512577	−0·50	—	—	—
Val3-2	Valcheta	52·5	0·704665	0·704630*	0·512605	0·512580	−0·45	18·628	15·641	38·659
Val3-4	Valcheta	52·2	0·704700	0·704665*	0·512591	0·512564	−0·76	—	—	—
Ang1A	Aguada Cecilio	—	0·704220	0·704185*	0·512632	0·512595	−0·15	18·297	15·600	38·339
Pat11A	Cari Laufquen	53·7	0·704586	0·704568*	0·512613	0·512582	−0·41	—	—	—
Pat11B	Cari Laufquen	53·3	0·704402	0·704386*	0·512619	0·512595	−0·16	—	—	—
Pat15A	Comallo	52·9	0·704961	0·704932*	0·512560	0·512524	−1·5	—	—	—
Pat15C	Comallo	53·7	0·705108	0·705075*	0·512525	0·512492	−2·2	18·419	15·625	38·471
Post-plateau flows				*at 20 Ma*		*at 20 Ma*				
TM1	Telsen	52·9	0·704525	0·704481*	0·512622	0·512609	−0·2	18·516	15·628	38·585
Ard 209	Telsen	53·0	0·704565	0·704531*	0·512638	0·512623	+0·12	—	—	—
Ard 58	Bajo Hondo	48·9	0·704359	0·704336*	0·512695	0·512680	+1·3	18·323	15·609	38·334
Ard 68	Bajo Hondo	49·7	0·704305	0·704282*	0·512711	0·512698	+1·7	—	—	—
GG9A	Gan Gan	51·9	0·704717	0·704680*	0·512629	0·512614	+0·04	18·148	15·574	38·242
M2A	near Maquinchao	48·3	0·704061	0·704044*	0·512748	0·512732	+2·3	18·570	15·640	38·538
M2B	near Maquinchao	48·8	0·704034	0·704018*	0·512758	0·512743	+2·6	—	—	—
M5	near Maquinchao	47·9	0·704120	0·704102*	0·512722	0·512708	+1·9	—	—	—
Quiñelaf intermediateto silicic volcanic rocks				*at 24 Ma*		*at 24 Ma*				
GG5	east of Gan Gan	59·0	0·704755	0·704647	0·512629	0·512613	0·11	18·359	15·617	38·432
GG4	east of Gan Gan	63·2	0·705013	0·704937*	0·512592	0·512576	−0·61	—	—	—
GG2	tuff near Gan Gan	71·2	—	—	0·512583	0·512566	−0·80	18·326	15·596	38·415
M12	Talagapa tuff	71·8	—	—	0·512564	0·512546	−1·2	—	—	—

*Initial $^{87}Sr/^{86}Sr$ ratios are based on Rb concentrations estimated from analyses of similar samples by Remesal (1988), Corbella (1989*a*), Corbella & Barbieri (1989), and Remesal *et al*. (2002). Sr/Rb ratios of these samples are all 25 or higher. Standards and analytical details are given in text; sample localities are given in Table A1.

(+4·6); and low $^{207}Pb/^{204}Pb$ and $^{208}Pb/^{204}Pb$ ratios at a given $^{206}Pb/^{204}Pb$ (18·7) ratio (Table 7; Figs 9 and 10). Their chemical characteristics generally resemble those of nearby Eocene back-arc flows (see Figs 7 and 9; Kay *et al.*, 1993, 2004) whose locations are shown in Figs 2b and 3. The Sierra de Chacays flows (CH1 in Fig. 5a) are similar to the Ranquil Huao flows in having high REE contents (Ce ~ 57 ppm), steep REE patterns (La/Yb = 15–18; La/Sm = 4·4–4·8), low $^{87}Sr/^{86}Sr$ ratios (0·7040), and high εNd (+2·1 to 2·6)

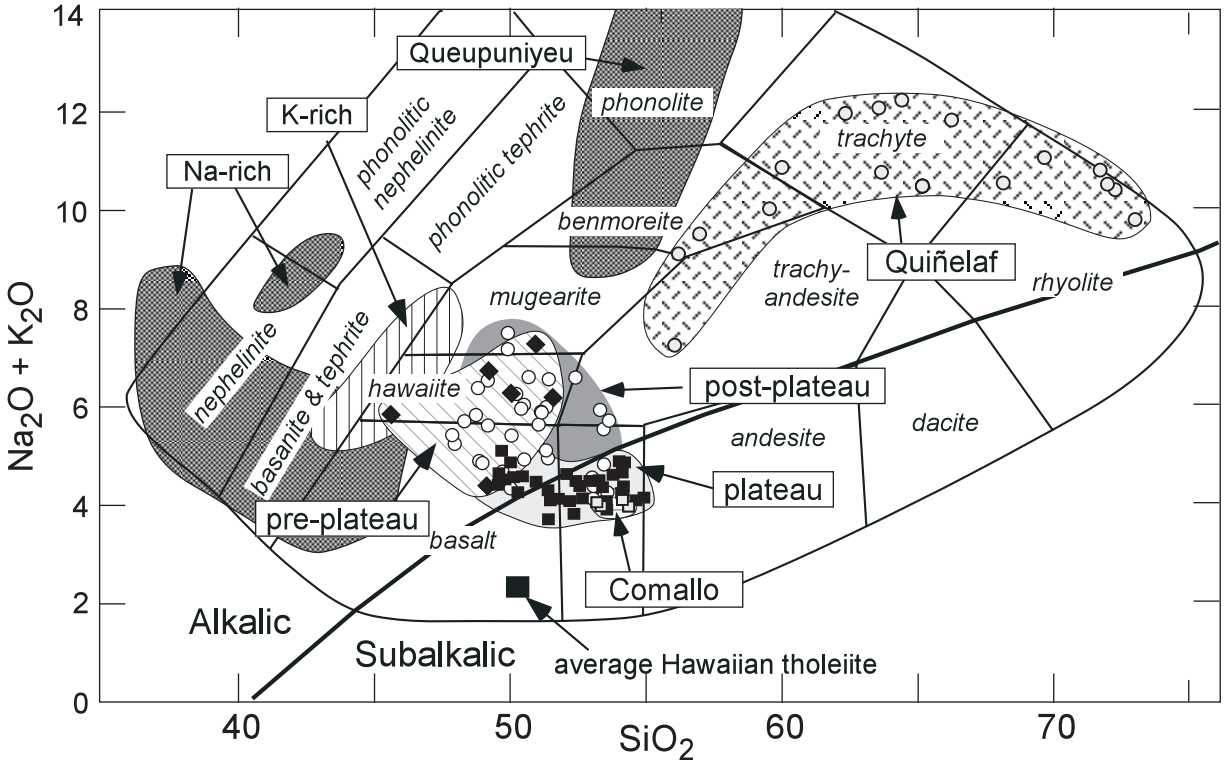

Fig. 4. Total alkalis ($Na_2O + K_2O$) vs SiO_2 (wt %) (TAS) showing late Oligocene to early Miocene Somuncura province pre-plateau, plateau, and post-plateau mafic lavas, intermediate to silicic volcanic rocks, and Na-rich and K-rich volcanic rocks relative to the TAS classification scheme of Le Bas & Streckeisen (1991) for alkaline igneous rocks. Data are from Tables 3–6, Electronic Appendix Tables 3–6 and Corbella (1982*b*, 1985, 1989*a*, 1989*b*). ♦, pre-plateau lavas; {□}, Comallo lavas; {■}, plateau lavas; {○}, post-plateau lavas; gray filled circles, silicic volcanic rocks.

values (Figs 5 and 9) compared with the overlying plateau flows.

Plateau flows

The plateau flows of the Meseta de Somuncura and surrounding mesetas, along with those in the Meseta de Canquel region, constitute the main volume of the Somuncura province and the main back-arc volcanism in Patagonia at this time (Figs 2 and 3). A relative contemporaneous volcanic lull from ~28 to 25 Ma to the west of the Somuncura province is consistent with the K/Ar ages for volcanic rocks in that region given by Cazau *et al.* (1987), Rapela *et al.* (1988) and Muñoz *et al.* (2000). As elsewhere in the Patagonia back-arc region, there is no structural evidence for significant extension in the Somuncura region at this time. In contrast, Muñoz *et al.* (2000) have argued for extension to the west in Chile during this period.

The Somuncura plateau group includes the voluminous basaltic to mafic andesitic flows in the Alta de Somuncura, Apas–Chacays–Telsen, and surrounding regions (Fig. 3). Ardolino & Franchi (1993) assigned late Oligocene to early Miocene ages to these flows based on a compilation of K/Ar ages that range from 33 ± 3 Ma to 22 ± 3 Ma for the mafic flows, and from 32 ± 2 Ma to 22 ± 2 Ma for associated trachytic and rhyolitic flows and sub-volcanic bodies. Remesal (1988) used many of the same K/Ar data to argue that Somuncura province volcanism climaxed in a 3 Myr period near 27 Ma. This proposal is consistent with paleomagnetic data from flows in the northeastern Meseta de Somuncura that fit the magmatic reversal record from ~27·5 to 25 Ma (Orgeira & Remesal, 1993). Evidence for contemporaneous volcanic activity in the Meseta de Canquel (Figs 1 and 2) comes from Deseadense (37–27 Ma) and Coluehuapense (25–23 Ma) mammal-bearing tuffs that bound a mafic volcanic sequence in which a flow yielded a K/Ar age of 27·9 ± 0·8 Ma (Marshall *et al.*, 1983, 1986).

Most of the Somuncura plateau flows appear to have erupted from large centers in the Apas–Chacays, the Alta de Somuncura, and the Carri Laufquen regions (Fig. 3). Constraints on the ages of the Apas–Chacays region centers come from flows in the Ranquil Huao region, where K/Ar ages range from 29 to 27 Ma (Ardolino & Franchi, 1993), and a flow near the top of the Ranquil Huao sequence that yielded a $^{40}Ar/^{39}Ar$

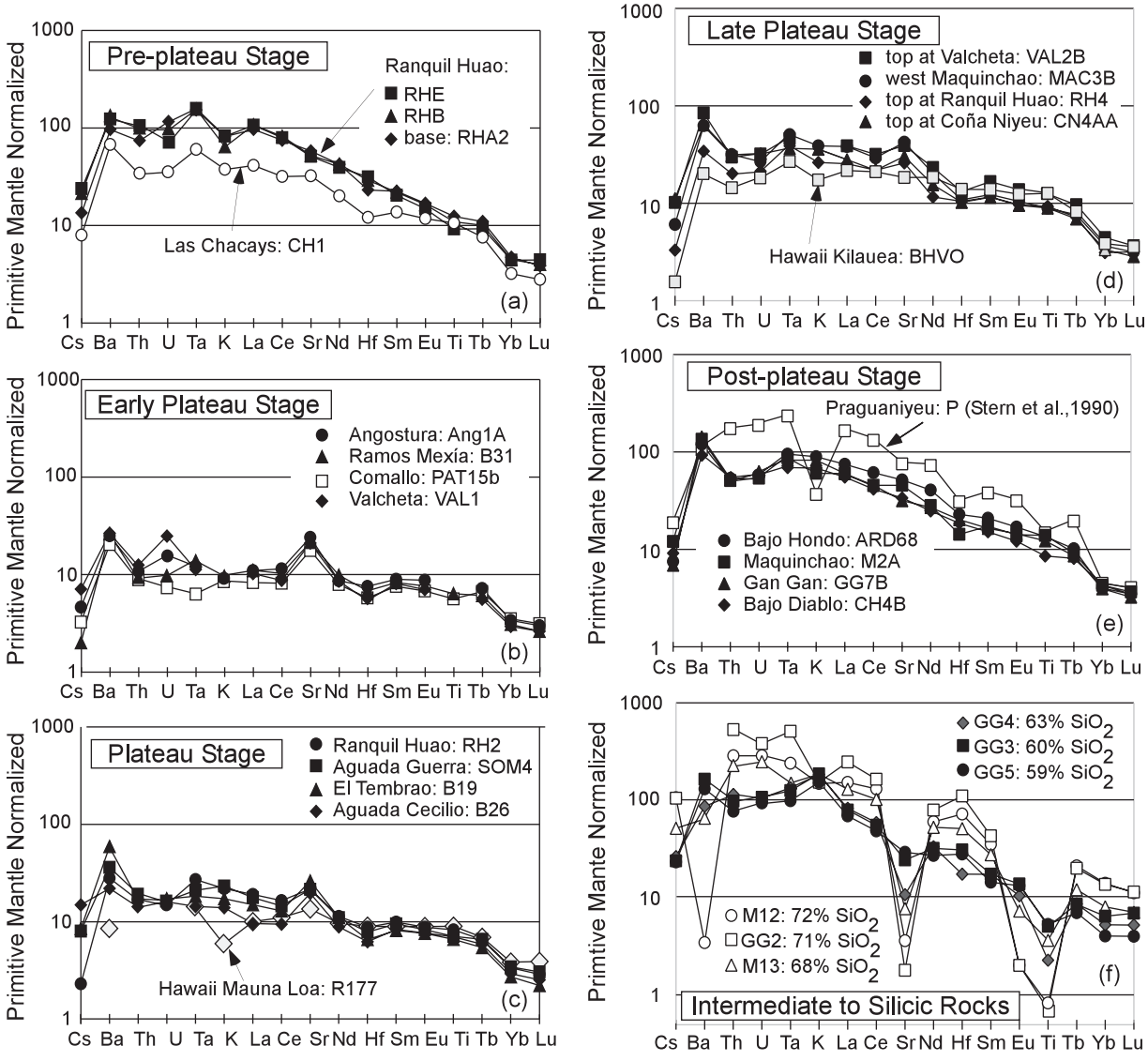

Fig. 5. Extended trace element plots for the Somuncura province volcanic rocks normalized to the primitive mantle values of Sun & McDonough (1989): Cs (0·032), Ba (6·989), Th (0·085), U (0·021), Ta (0·041), K (33·2), La (0·687), Ce (1·775), Sr (21·1), Nd (1·354), Hf (0·309), Sm (0·444), Eu (0·168), Ti (4·61), Tb (0·108), Yb (0·493) and Lu (0·074). Data for Somuncura province samples are from Tables 3–6, for the Praguaniyeu sample from Stern *et al.* (1990), and for Hawaiian Mauna Loa tholeiite R117 from Yang *et al.* (1996). Data for Kilauea basalt (Hawaii) are from INAA analyses of USGS standard BHVO at Cornell University (see analytical methods).

total-fusion age of 26·9 ± 0·8 Ma (Table 2). K/Ar ages for flows in the Alta de Somuncura region mostly range from 26 to 24 Ma (Ardolino & Franchi, 1993). Those in the Meseta de Carri Laufquen region are 31 ± 2, 28 ± 2, and 24 ± 5 Ma (Coira *et al.*, 1985).

The plateau sequences are dominated by olivine–clinopyroxene–plagioclase-bearing basaltic and orthopyroxene-bearing basaltic andesitic flows that are distinct in their major and minor element chemistry from the pre-plateau flows (Table 4). Overall, the plateau flows have transitional alkaline to subalkaline compositions with 49·2–54·5% SiO_2 (Fig. 4). Among their distinctive features are relatively high FeO*/MgO ratios (1·5–2·4), low MgO (4·3–8·5%), Cr (most 130–380 ppm), and Ni (90–210 ppm) concentrations, high Sr (most 400–500 ppm) and Na_2O (3·4–4·3%) concentrations, and small to absent Eu anomalies. Other differences from the pre-plateau flow include lower LREE abundances (Ce = 14–60 ppm) and flatter overall and LREE slopes (La/Yb = 3–15; La/Sm = 1·6–4·7) (Figs 5b–d and 6). Further contrasts are higher ratios of alkali/alkaline earth elements relative to REE and HFSE, with some flows having notably higher Sr/La (25–70, most >26), Ba/La (14–38, most >18), Ba/Ta

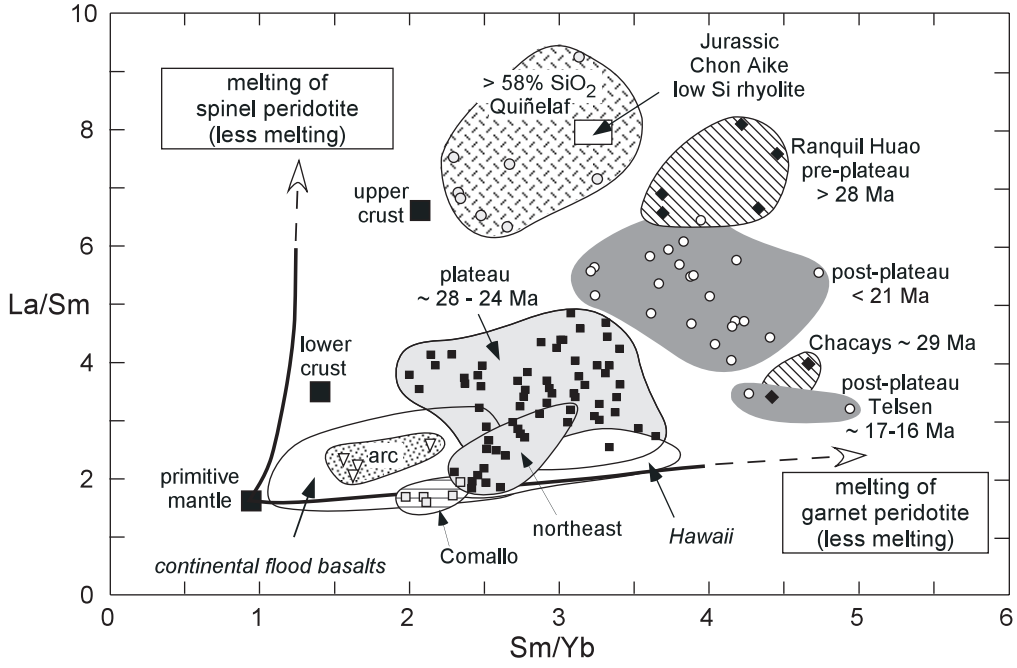

Fig. 6. La/Sm vs Sm/Yb showing fields for Somuncura province pre-plateau, plateau, and post-plateau mafic flows and intermediate to silicic volcanic rocks. Fields for plateau lavas near Comallo, and distal flows in the northeastern part of the Meseta de Somuncura (labeled northeast) are indicated. Also shown are the field (stippled) for Paleogene to Miocene arc rocks (Kay & Rapela, 1987; Kay *et al.*, 1993) and the average composition of the Jurassic Chon Aike low-SiO_2 rhyolite (Pankhurst & Rapela, 1995; Table 6). Comparative fields for Hawaiian and continental flood basalts are from Lassiter & DePaolo (1997). Average bulk continental upper crust and lower crust compositions are from Rudnick & Fountain (1995) and the primitive mantle composition is from Sun & McDonough (1989). Curves emanating from primitive mantle are trends for magmas resulting from decreasing degrees of melting of spinel and garnet peridotite mantle sources from Lassiter & DePaolo (1997). Symbols and data sources are as in Fig. 4.

(190–710), La/Ta (10–24), and Th/Ta (1·2–2·5) (Fig. 7). Isotopic differences include higher $^{87}Sr/^{86}Sr$ ratios (0·7043–0·7051), lower εNd values (+1·2 to +2·2), and slightly higher $^{207}Pb/^{204}Pb$ and $^{208}Pb/^{204}Pb$ ratios at a given $^{206}Pb/^{204}Pb$ ratio (Table 7; Figs 9 and 10).

Several features of the plateau group are noteworthy. First, where stratigraphic relations are clearest, the younger (late plateau) flows tend to have steeper LREE patterns, and slightly lower $^{87}Sr/^{86}Sr$ ratios than the older (early and main plateau) flows (Figs 5 and 9). Second, long early and main plateau flows that reach the northern margin of the plateau (e.g. at Aguada Cecilio; Fig. 3) tend to have the flattest LREE and steepest heavy REE (HREE) slopes (La/Sm = 1·6–2·2; Sm/Yb ratios = 1·9–2·6; Figs 5b, c and 6), highest $^{87}Sr/^{86}Sr$ ratios, and lowest εNd values (Fig. 9) in the Somuncura region. REE patterns like these are uncommon in continental alkali lavas, but are found in oceanic hotspot lavas such as those from Hawaii (Figs 5b and 6). Third, Comallo region flows, which are the furthest west and closest to the modern Southern Volcanic Zone (SVZ) arc (Fig. 3), are notable for their flat LREE patterns (La/Yb = 3–4, La/Sm = 1·6–1·9: Figs 5b and 6), high La/Ta ratios (18–24: Fig. 7), high $^{87}Sr/^{86}Sr$ ratios (0·7050–0·7051) and low εNd (–1·5 to –2·2) (Fig. 9).

Post-plateau flows

The post-plateau flows erupted in the nearly orthogonal convergence regime that emerged after the breakup of the Farallón plate (e.g. Pardo-Casas & Molnar, 1987). According to Somoza (1998), the Nazca plate had a convergence vector of ~80° NE with the South American plate and the convergence velocity was ~16 cm/yr at this time. Published K/Ar age data are consistent with contemporaneous arc volcanism being present to the west after ~25 Ma with eruptions in the Ventana belt in Argentina (~25–24 Ma; Cazau *et al.*, 1987; Rapela *et al.*, 1988) and in Chile (~25–20 Ma; Muñoz *et al.*, 2000). Widespread back-arc volcanism also took place to the north and south (Figs 1 and 2). To the north between 36° and 38°S, 24–20 Ma alkali olivine basalt flows were followed by 19–16 Ma basaltic andesitic to dacitic volcanic centers (Kay & Copeland, 2006). To the south, mafic flows with K/Ar ages of 22·1–19·6 Ma are found in the Meseta de Canquel (Marshall *et al.*, 1986). Early Miocene extension to the west has been suggested based on studies of sedimentary and volcaniclastic sequences in the Cura Mallin basin near 36° to 39°S (Jordan *et al.*, 2001), sedimentary sequences in the Nirihuau basin (Fig. 2b), where subsidence has been shown to peak during a marine

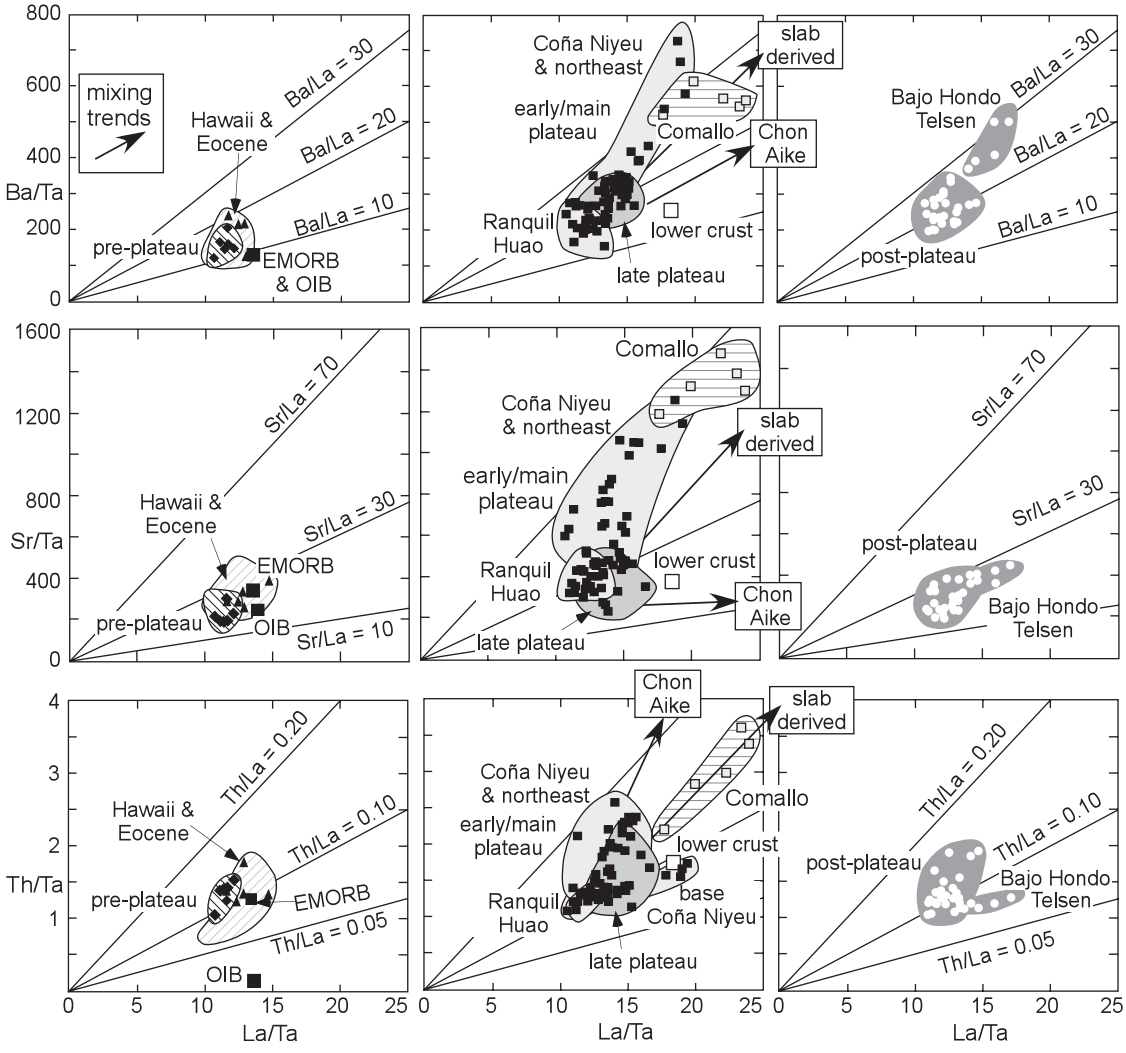

Fig. 7. Variation of Ba/Ta, Sr/Ta, and Th/Ta vs La/Ta for the Somuncura province pre-plateau, plateau and post-plateau mafic volcanic rocks (symbols are as in Fig. 4). Labeled fields are for specific localities discussed in the text. Shown for comparison are fields for Somuncura region Eocene back-arc and Hawaiian mafic volcanic rocks. Arrows show mixing trends for Somuncura pre-plateau (or Eocene or Hawaiian) mafic lavas with slab-derived components and average Chon Aike low-SiO_2 rhyolite. The Eocene field is based on data from Kay *et al.* (1993, 2002, 2004) for samples from the Cerro El Buitre, Cerro Mendive, El Sombrero, El Cain and Cerro Cortado localities (Figs 2b and 3). Hawaiian data are from Watson (1993) and Yang *et al.* (1996). E-MORB and OIB compositions are from Sun & McDonough (1989). Average crustal compositions are from Rudnick & Fountain (1995) with the upper crustal Ta concentration from Plank & Langmuir (1998). Ratios for the Chon Aike rhyolite (La/Ta = 37; Ba/Ta = 542; Sr/Ta = 227; Th/Ta = 8·8; sample 453 in Table 6) and upper crust (La/Ta = 31; Ba/Ta = 561; Sr/Ta = 357; Th/Ta = 11) extend off the diagram. The distinctive high Ba/Ta, Sr/Ta and Th/Ta ratios of the plateau flows relative to the pre- and post-plateau flows should be noted. (See discussion in text.)

ingression (Cazau *et al.*, 1987), and volcanic and sedimentary sequences in Chile (Muñoz *et al.*, 2000). The amount of extension is still the subject of debate.

The post-plateau flow sequences are more restricted in volume and distribution than the plateau flows. They are concentrated in a NW–SE-trending band that runs from the Meseta Carri Laufquen to the Telsen region along the western and southern margins of the Meseta del Somuncura (Fig. 3). Ardolino & Franchi (1993) assigned most of these flows to the early Miocene based on a compilation of K/Ar ages that range from 23·3 ± 2 to 15 ± 1 Ma. Coira *et al.* (1985) reported a K/Ar age of 20 ± 1 Ma on a flow in the Meseta de Carri Laufquen. These age assignments agree with the two new total-fusion $^{40}Ar/^{39}Ar$ ages in Table 2. The 20·6 ± 0·6 Ma age is from a flow SE of Maquinchao. The 16·6 ± 0·4 Ma age is from a flow in the Telsen region near where K/Ar ages of 17 ± 1 Ma and 15 ± 1 Ma have been reported previously (see Ardolino & Franchi, 1993). The post-plateau stage ended with the eruption of the Telsen region flows.

The olivine–plagioclase-bearing mafic post-plateau flows largely have alkali basaltic, trachybasaltic,

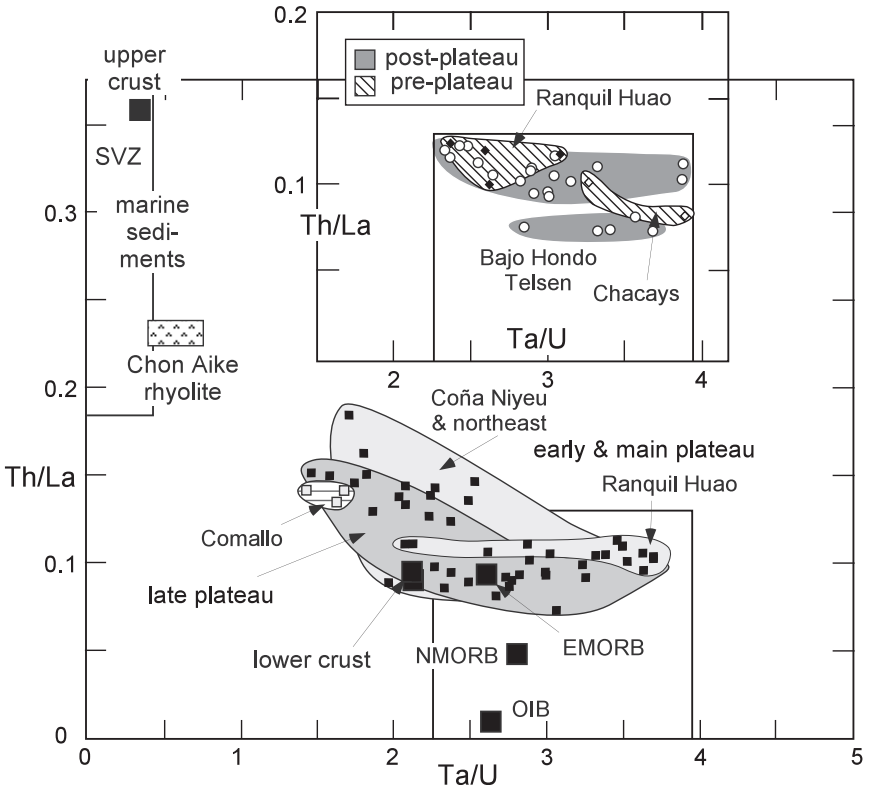

Fig. 8. Th/La vs Ta/U for the Somuncura province volcanic rocks. Only samples with Th/U ratios in the range 3–5·5 are plotted to minimize the effects of U mobility that could be attributable to secondary processes. Ratios for N-MORB, E-MORB and OIB are from Sun & McDonough (1989) and for upper and lower crust from Rudnick & Fountain (1995). The Southern Volcanic Zone (SVZ) arc field (rectangular box in upper left) is based on data from Hickey *et al.* (1986) and Hildreth & Moorbath (1988). The marine sediment region is from Klein & Karsten (1995). It should be noted that ratios for the pre- and post-plateau flows are closer to MORB than those for the plateau flows, which extend towards the arc–continental crust region. Symbols and other data sources are as in Fig. 4.

mugearitic and hawaiitic compositions (Fig. 4). Compared with the plateau flows, they are generally characterized by lower SiO_2 (most 48–52%), MgO (3·7–5·2%), Cr (most 3–250 ppm) and Ni (most 25–45 ppm), and higher TiO_2 (most 2–3·3%) and K_2O (most 1·9–2·7%) contents (Table 5). They also have higher incompatible element abundances (Ce ~ 55–110 ppm); steeper REE patterns (La/Yb ~ 15–26; La/Sm ~ 4–7) (Figs 5e and 6); and generally similar Ba/La (19–31), Ba/Ta (240–500), and La/Ta (10–16) ratios along with lower Sr/La (15–30) ratios (Fig. 7). In addition, their $^{87}Sr/^{86}Sr$ ratios range to lower values (most are 0·7040–0·7045), their εNd (–0·2 to +2·3) to higher values, and their Pb isotopic ratios overlap (Table 7; Figs 9 and 10). They differ from the pre-plateau flows in being more Na_2O- and less K_2O-rich (Table 3). They also have lower La/Sm ratios than the pre-plateau Ranquil Huao flows (Fig. 6), higher Sr/La, Ba/Ta, and Ba/La ratios and a greater range of La/Ta ratios (Fig. 7), and lower $^{87}Sr/^{86}Sr$ ratios and higher εNd values (Fig. 9).

Intermediate and silicic volcanic rocks

More silicic volcanic rocks that are temporally and spatially related to the mafic lavas include trachytic to comenditic rhyolitic tuffs, benmoreite to mugearite domes, and subvolcanic intrusive rocks (Fig. 4; Corbella, 1982*a*, 1982*b*, 1984; Ardolino, 1987; Remesal, 1988; Corbella, 1989*a*). They are most abundant in the Sierras de los Chacays, Telsen, Apas, Talagapa, and Alta Sierra de Somuncura regions (Fig. 3), where they seem to be associated with large eruptive centers (Corbella, 1984). Compiled K/Ar ages for silicic tuffs and domes in the Sierras de Apas and Chacays regions range from 31 ± 2 to 25 ± 5 Ma and coincide with those of the plateau flows. K/Ar ages for trachytic tuffs and domes near Telsen range from 22 ± 2 to 18·2 ± 2 Ma and coincide with those of post-plateau flows in that region (Corbella, 1982*a*, 1982*b*; Ardolino & Franchi, 1993).

New chemical and Sr–Nd–Pb isotopic data (Tables 6 and 7) for samples with 59–71% SiO_2 from south of the Sierra de Apas and the Talagapa region (Fig. 3) supplement major and trace element analyses by

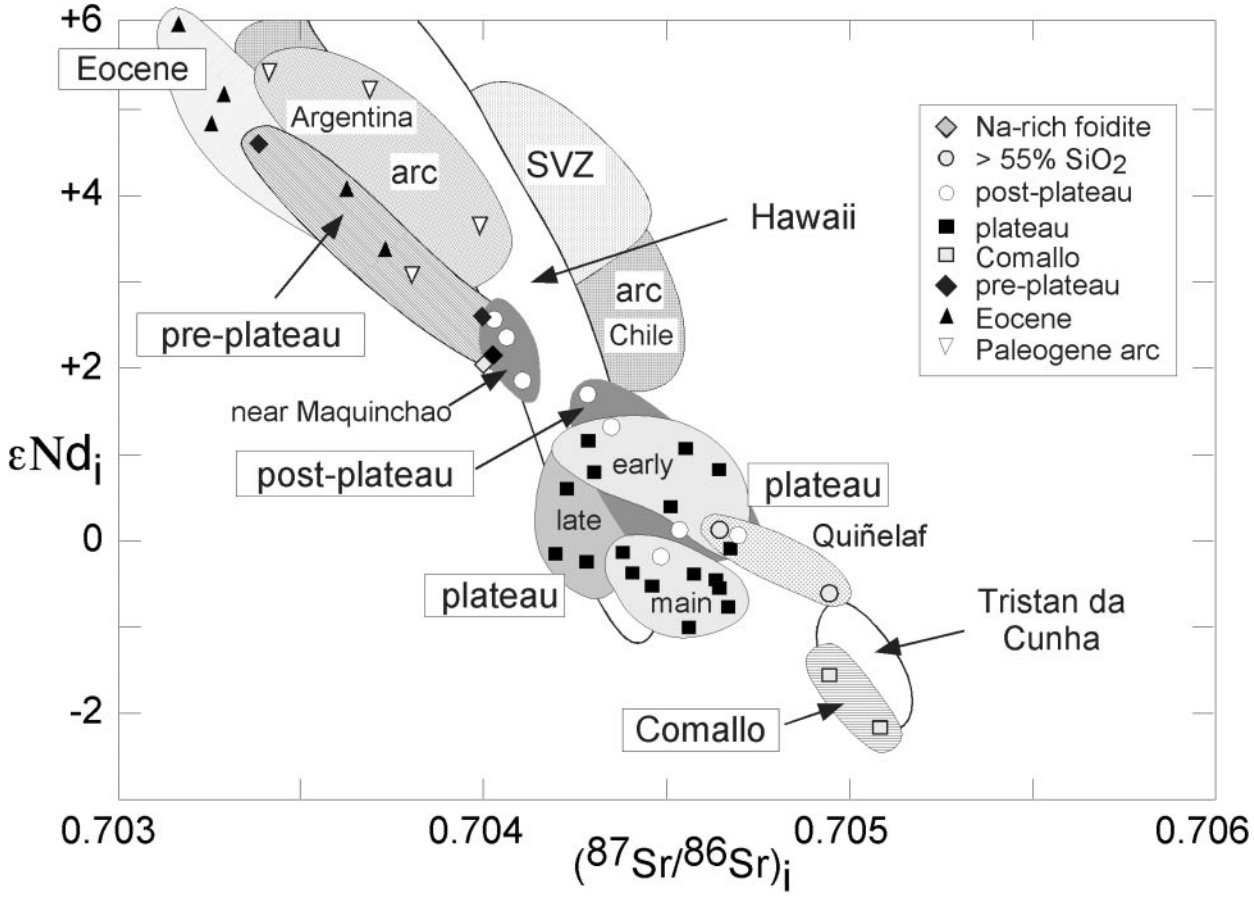

Fig. 9. Variation of initial εNd vs initial $^{87}Sr/^{86}Sr$ for the Somuncura province volcanic rocks compared with those for Paleogene to early Miocene arc rocks in Argentina and Chile, the modern Southern Volcanic Zone (SVZ) arc and oceanic intraplate lavas from Hawaii and Tristan da Cunha. Data for Somuncura samples are from Table 7. Data for Eocene back-arc and Tertiary arc lavas in Argentina are from Kay *et al.* (1993, 2002, 2004) and Electronic Appendix Table 5. The Tertiary arc field in Chile is based on data from Munoz *et al.* (2000) and the SVZ field is based on data of Hickey *et al.* (1986) and Hildreth & Moorbath (1988). Fields for Hawaii and Tristan de Cunha were compiled by Paslick *et al.* (1995). Somuncura data are from Table 7. Praguaniyeu foidite data are from Stern *et al.* (1990).

Corbella (1982*b*, 1984, 1989*a*). Mineralogical characteristics described by Corbella (1982*b*, 1984, 1989*a*) and total alkali vs SiO_2 and trace element characteristics shown in Figs 4 and 5f are like those in other alkaline continental and oceanic intraplate volcanic rocks. Particularly distinctive among their trace element characteristics are high REE, Th, U and Ta contents, low Sr and Ba contents, and negative Eu anomalies that reach an extreme in the trachytic tuffs (Fig. 5f and Table 6). Initial Pb, Sr, and Nd isotopic ratios of a benmoreite with 59% SiO_2 (GG5 in Table 6) overlap those of the mafic plateau flows (Figs 9 and 10), as do the Pb isotopic ratios of a trachytic tuff with 71% SiO_2 (GG2; Table 6). Initial εNd values of four samples (Table 7) decrease slightly (+0·1 to −1·2) with increasing SiO_2 (59–72%). It is not possible to calculate initial $^{87}Sr/^{86}Sr$ in samples with >71% SiO_2 because of high Rb/Sr ratios (>100) and imprecise ages.

High-potassium and sodium-rich flows

Other Somuncura province region volcanic rocks include K-rich lavas with orenditic (47% SiO_2, 5·5–7% K_2O, 7–8% MgO) to latitic (60–67% SiO_2) compositions that erupted at the southern margin of the Sierra de Chacays at Plan-Luan (Corbella, 1983, 1989*a*), nephelinitic to phonolitic lavas in the Sierra de Queupuniyeu and Praguaniyeu regions (Corbella, 1982*c*, 1983, 1989*b*), and nephelinitic lavas in the Alta Sierra de Somuncura (Corbella, 1985; Fig. 3). Few trace element and isotopic data are available for these rocks. An early Miocene age for the high-K volcanic rocks is based on a 19·3 ± 3 Ma whole-rock Rb–Sr date that puts their initial $^{87}Sr/^{86}Sr$ ratio between 0·7058 and 0·7065 (Corbella & Barbieri, 1989). An early Miocene age for the sodic nephelinite, basanite, phonolitic tephrite, and aegerine–augite and analcime-bearing phonolite flows in the Sierra de Queupuniyeu area is based on a K/Ar age of 19·3 ±

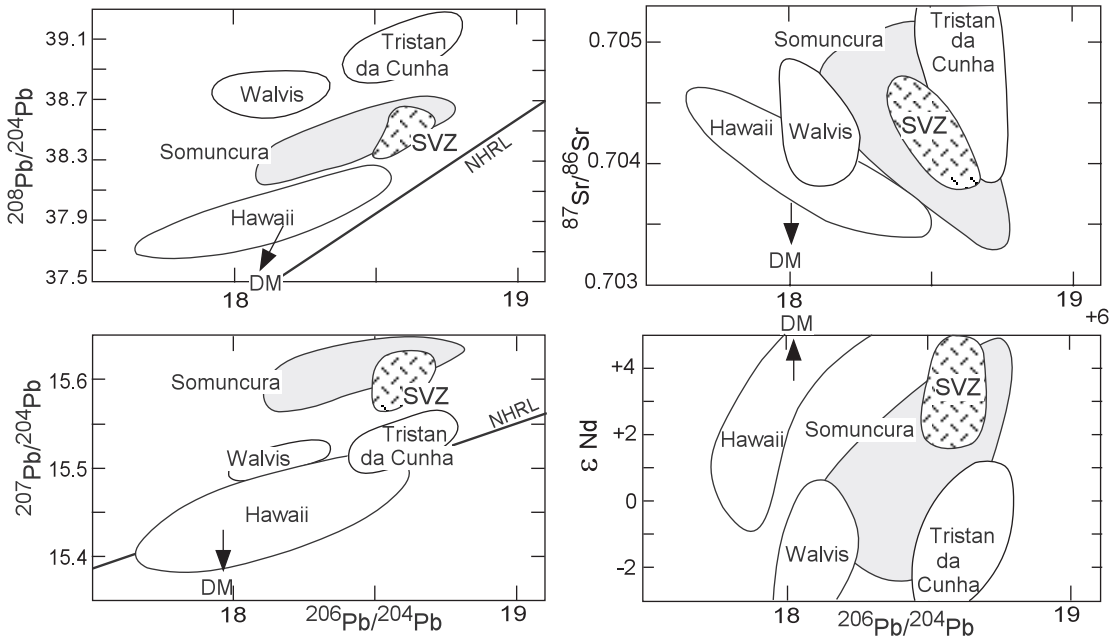

Fig. 10. Variation of initial εNd, $^{87}Sr/^{86}Sr$, $^{207}Pb/^{204}Pb$ and $^{208}Pb/^{204}Pb$ vs $^{206}Pb/^{204}Pb$ for the Somuncura province volcanic rocks and comparative fields for the SVZ (Hickey *et al.* 1986; Hildreth & Moorbath, 1988), Tristan da Cunha and Walvis Ridge (compilation from Ewart *et al.*, 2004) and Hawaiian (compilation from Paslick *et al.*, 1995) volcanic rocks. (See text for discussion.) Symbols and data sources are as in Fig. 9. NHRL, Northern Hemisphere Reference Line of Hart (1984).

1 Ma on a basanite flow (Corbella, 1982*c*). An undated Praguaniyeu nephelinite (39% SiO_2) analyzed by Stern *et al.* (1990) has high La/Yb (51, Fig. 5) and low Ba/La (6·5) and La/Ta (12), and Sr–Nd–Pb isotopic ratios similar to those of the post-plateau mafic lavas (Figs 9 and 10). A garnet lherzolite xenolith from a Praguaniyeu flow yielded a Sm–Nd mineral isochron age of 29·4 ± 5·7 Ma (Bjerg *et al.*, 2005).

DISCUSSION: ORIGIN OF THE SOMUNCURA PROVINCE MAGMATIC ROCKS

Understanding the origin of the Somuncura province magmas requires deconvolving their mantle and crustal components, source melting conditions, and ascent paths. The approach below is to evaluate first the role of crustal contaminants, then that of pre-existing lithosphere and subducted components, and finally that of asthenospheric components. Temporal and spatial changes are used as tools in differentiating crustal and mantle components, and major and trace element data in evaluating mantle melting percentages and depths. Comparisons with Hawaiian intraplate magmas are used to evaluate the role of an oceanic intraplate-like asthenospheric upwelling and the differences that can be explained by subducted components. Finally, the tectonic setting of the Somuncura province is reappraised in terms of local and regional constraints.

Role of crustal contaminants

A question that arises for mantle-derived magmas that are erupted through continental crust is the extent to which these magmas are affected by crustal contaminants. Intraplate-like Th/La and Ta/U ratios (Fig. 8) and relatively low $^{87}Sr/^{86}Sr$ ratios and high εNd values (Fig. 9) like those in the Somuncura province pre- and post-plateau mafic lavas are generally taken as evidence against significant upper crustal contamination. In contrast, a number of the chemical characteristics of the plateau lavas could imply a larger role for crustal contamination. Relative to the pre- and post-plateau lavas, the plateau lavas have higher $^{87}Sr/^{86}Sr$ ratios and lower εNd values (Fig. 9), higher SiO_2 contents (up to 53%; Fig. 4), higher large ion lithophile element (LILE)/REE ratios (e.g. Sr/La, Ba/La and Th/La ratios, Fig. 7) and an upper crustal contamination trend on a Ta/U vs Th/La plot (Fig. 8). At the same time, restrictions on the amounts of crustal contaminants in the plateau lavas come from their high MgO (6·8–7·8%), Cr (250–330 ppm), and Ni (180–210 ppm) contents, low LREE contents, flat light and steep HREE patterns, limited

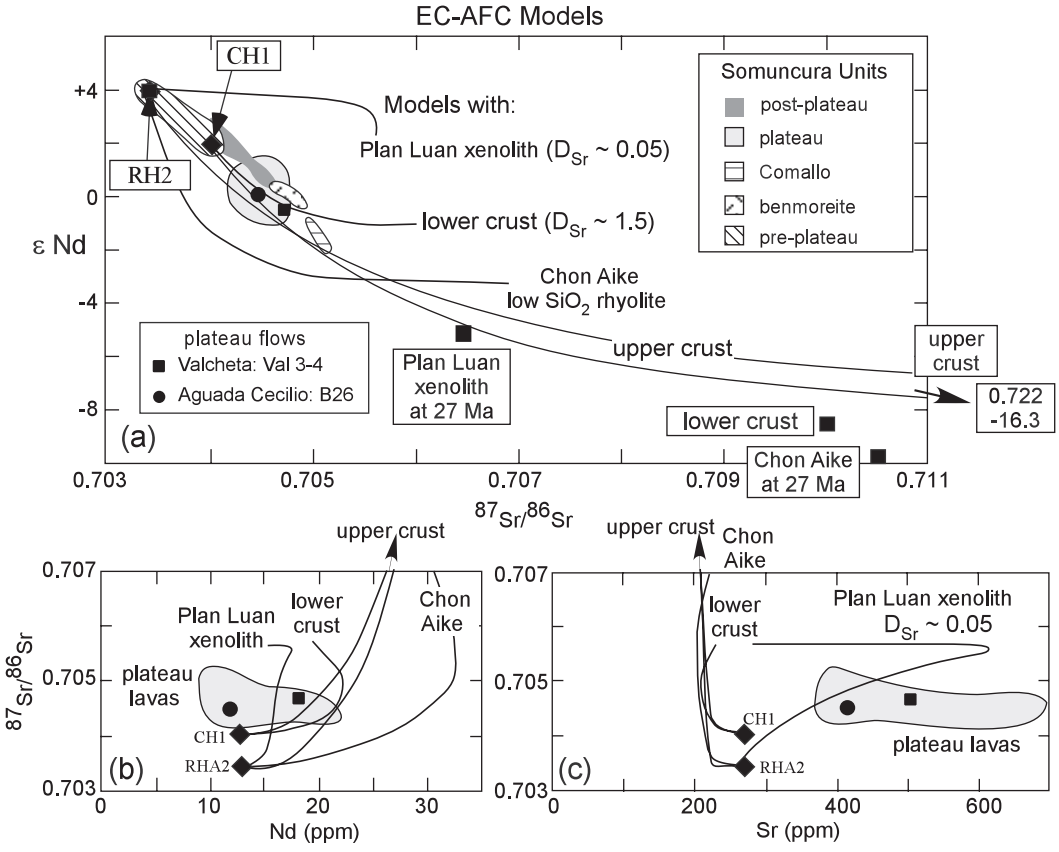

Fig. 11. Variation of: (a) $^{87}Sr/^{86}Sr$ vs εNd, (b) $^{87}Sr/^{86}Sr$ vs Nd (ppm) and (c) $^{87}Sr/^{86}Sr$ vs Sr (ppm) showing results of EC-AFC (energy constrained assimilation–fractional crystallization) modeling (Spera & Bohrson, 2001) for mantle-derived basalts and crustal contaminants compared with Somuncura plateau lavas. Trace element contents in the modeled mantle-derived magma are based on Hawaiian tholeiitic basalt R117 (Rhodes, 1996; Yang *et al.*, 1996); and $^{87}Sr/^{86}Sr$ and $^{143}Nd/^{144}Nd$ are from the pre-plateau basalts RHA2 and CH1 (Table 7). Trace elements for the modeled crustal assimilants are based on Chon Aike low-SiO_2 rhyolite 453 (Table 6), Plan-Luan lower crustal xenolith Chacays 2 (Pankhurst & Rapela, 1995) and the upper and lower crustal averages of Rudnick & Fountain (1995). Nd–Sr isotopic ratios for the Chon Aike low-SiO_2 rhyolite sample Con89-42 and the Plan-Luan xenolith sample Chacays 2 recalculated to 27 Ma are from Pankhurst & Rapela (1995). All concentrations, isotopic ratios and temperatures used in the models are listed in Table A2.

HFSE depletion (e.g. low La/Ta ratios), and relatively high Sr contents.

Possible upper crustal contaminants in the plateau magmas are the voluminous Jurassic Chon Aike rhyolitic and related magmatic rocks that were emplaced during a massive regional crustal melting event preceding and accompanying the opening of the South Atlantic Ocean (e.g. Kay *et al.*, 1989; Pankhurst & Rapela, 1995). Support for contamination from these rhyolites comes from the presence of aggregates of corroded quartz and partially digested feldspar in the plateau lavas (Remesal & Parica, 1989). The studies of Rapela & Pankhurst (1993) and Pankhurst & Rapela (1995) show that two varieties of Chon Aike volcanic rocks (Table 6) are common in the Somuncura region. The first is a high-SiO_2, LILE-depleted rhyolite with a very large negative Eu anomaly and an age-corrected $^{87}Sr/^{86}Sr$ ratio >0·760 at 27 Ma, and the second is a low-SiO_2, more LILE-rich rhyolite with a $^{87}Sr/^{86}Sr$ ratio near 0·710 at 27 Ma. The high-SiO_2 rhyolite could have played a role in elevating the SiO_2 contents of the plateau lavas, but could not have had much effect on their LILE contents or $^{87}Sr/^{86}Sr$, Ba/La, and Ba/Ta ratios based on mass-balance considerations.

Isotopic and trace element considerations indicate that neither the low-SiO_2 Chon Aike rhyolite nor any average upper crustal assimilant is likely to have played a major role in shaping the distinctive LILE/REE ratios and isotopic characteristics of the plateau lavas. The first-order problems with upper crustal contaminants emerge in both simple mixing models and energy-constrained assimilation and fractional crystallization (EC-AFC) models that use the formulation of Spera & Bohrson (2001). The mantle-derived basalts used in the models are assumed to have the isotopic ratios of the pre-plateau lavas;

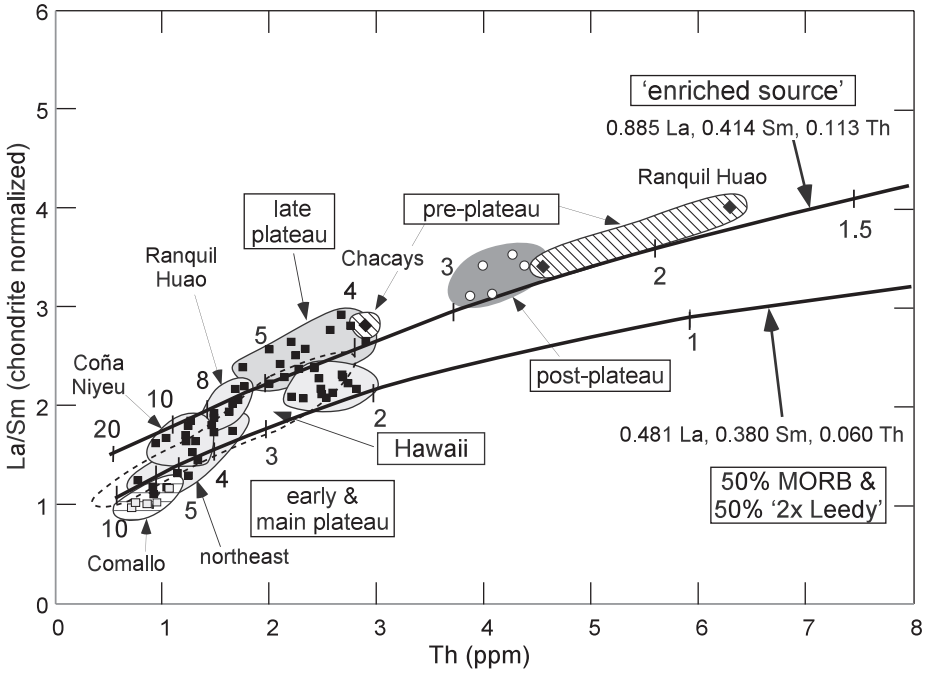

Fig. 12. Th concentration (ppm) vs La/Sm ratio normalized to Leedy chondrite abundances (La = 0·378 ppm, Sm = 0·23 ppm; Masuda *et al.*, 1973) for Somuncura province mafic volcanic samples with Cr >250 ppm compared with calculated partial mantle melting models for Patagonian back-arc magmas from Gorring & Kay (2001). The models are for non-modal incremental batch melting of an 'enriched' source (La = 0·885, Sm = 0·414, Th = 0·113 ppm), and a more depleted source that is a mixture of 50% MORB and 50% mantle with a composition of two times Leedy chondrite (La = 0·481 ppm, Sm = 0·380 ppm, Th = 0·060 ppm). Tick marks indicate per cent of melting. As in the study by Plank & Langmuir (1992), the models assume small melt increments (0–5%) in a vertical melting column with all melts pooled at the top of the column. Details of the models have been given by Gorring & Kay (2001). Labeled fields are those discussed in the text. Comparative field for Hawaiian samples (dashed line) is based on data from Chen & Frey (1985) and Yang *et al.* (1996). Symbols and data sources are as in Fig. 4. (See text for discussion.)

however, as the pre-plateau lavas have high LILE concentrations and steep REE patterns, their trace element characteristics are inappropriate. As no suitable basalt is known in the Somuncura region, the trace element concentrations of a primitive Hawaiian tholeiite (R117 of Yang *et al.*, 1996) whose flat LREE and steep HREE patterns approach those of the plateau lavas like B26 are used (Fig. 5c).

Illustrative simple mixing models (not shown) that combine ~80–85% of this basaltic end-member with 15–20% of the low-SiO_2 Chon Aike rhyolite approach the $^{87}Sr/^{86}Sr$ ratios (~0·7047), εNd, and Th, K, and REE contents of plateau lavas such as VAL3-4, but fail to match their relatively high Sr, Ba and Ta contents. These models can be improved by using more Sr, Ba and Ta-rich basalts, but none of them simultaneously match the REE, Ta, and Th contents or the trends of Ba/Ta, Ba/La and Th/Ta ratios in the early and main plateau lavas (Fig. 7).

More complex isotopic and trace element EC-AFC models that allow for selective enrichment of incompatible elements are not any more successful (Fig. 11). The problem is that these models do not explain why Ba, Sr and Ta are enriched in the plateau lavas, whereas the REE are not. Another problem is that plateau lavas like B-26, which have high $^{87}Sr/^{86}Sr$ and low Sr contents, show the least evidence for LILE contamination. The failure of the EC-AFC models can be seen in the various plots in Fig. 11. Models that produce Sr and Nd isotopic trends like those in the Somuncura lavas (Fig. 11a) fail by overestimating Nd (Fig. 11b) and Th concentrations, and severely underestimating Sr (Fig. 11c) concentrations in plateau lavas such as Val3-4 and B26. Parental basalts similar to the average enriched mid-ocean ridge basalt (E-MORB) and ocean island basalt (OIB) of Sun & McDonough (1989), with lower Sr contents, produce even worse matches. As such, models that explain higher $^{87}Sr/^{86}Sr$ ratios and lower $^{143}Nd/^{144}Nd$ in the plateau lavas than in the pre- and post-plateau lavas by adding Chon Aike or upper crustal contaminants are inconsistent with LILE distributions.

Three other observations also point to the differences among the Somuncura province lavas as being primarily due to other factors. The first is that Eocene and pre-plateau lavas that erupted though the same crust as the plateau lavas lack their high, arc-like Ba/La and Sr/La ratios. These high Ba/La and Sr/La ratios are also absent in plateau lavas that erupted through a similar

type of crust east of the Chile Triple Junction to the south (Fig. 1; Ramos & Kay, 1992; Gorring *et al.*, 1997). The second is that a virtual overlap in $^{87}Sr/^{86}Sr$ and $^{143}Nd/^{144}Nd$ ratios in mafic and silicic Somuncura province volcanic rocks (Fig. 9) is inconsistent with a Chon Aike rhyolite contaminant shaping the properties of the silicic magmas. A similar case can be made for overlapping $^{87}Sr/^{86}Sr$ ratios in Plan-Luan region orenditic (0·7058–0·7066, ~47% SiO_2, >5% K_2O) and K-latitic (0·7062–0·7067; 60–67% SiO_2) volcanic rocks (Corbella & Barbieri, 1989). The third is that the high K/Na ratios in the high-K mafic to silicic Plan-Luan region volcanic rocks contrast with the high Na/K ratios in nephelinite to phonolitic lavas elsewhere in the region (Corbella, 1984). This contrast implies that mantle, rather than crustal components shape the chemical differences between these sequences.

Another issue is the role of lower crustal contaminants in the petrogenesis of the plateau magmas. The relatively high FeO*/MgO ratios (1·5–2·4) and relatively low MgO (4·3–8·5%), Cr (most 130–380 ppm), and Ni (90–210) contents of the plateau lavas are pertinent in that they indicate that the magmas have fractionated olivine and clinopyroxene. Likewise, high Sr (most 400–500 ppm) and Na_2O (3·4–4·3%) contents and small negative Eu anomalies fit with minimal plagioclase removal. Along with the petrographic features summarized by Remesal (1988), these characteristics indicate crystallization of olivine and pyroxene before plagioclase, as expected in mafic magmas that fractionate at deep crustal levels where they could assimilate lower crust. Importantly, an approximation of the lower crustal composition in the region comes from granulite xenoliths in the Plan-Luan potassic volcanic rocks that Pankhurst & Rapela (1995) argued have the depleted chemistry (Nd <5·5 ppm; Rb <2 ppm; Sr ~550–750 ppm; $^{87}Sr/^{86}Sr$ ratios = 0·7065–0·7078; $\varepsilon Nd = -3$ to $-6{\cdot}10$) expected of lower crust that is residual to the Chon Aike rhyolites. EC-AFC models that use the same basaltic end-member as in the upper crustal models above and the parameters in Table A2 (see the Appendix) show that assimilants like the Plan-Luan xenoliths and generic lower crust also fail to produce the distinctive isotopic and trace element characteristics of the plateau lavas. As shown in Fig. 11, best-fit models that use Sr distribution coefficients near 0·05, which are in accord with plagioclase instability, produce Sr concentrations that approach those in the plateau lavas, but fail to match their Nd and Sr isotopic ratios (e.g. model with Plan-Luan xenolith in Fig. 11). Models that use higher Sr distribution coefficients (~1·5) produce a better match for the Sr and Nd isotopic characteristics of the plateau lavas, but fail to produce their high Sr concentrations (see model with lower crust in Fig. 11a and c).

Role of subducted contaminants

The presence of subducted components in the mantle source can explain why Ba/Ta, Sr/Ta, Th/Ta, Ba/La, Sr/La, and Th/La ratios in the plateau lavas are higher than those in MORB and intraplate (OIB) lavas (Fig. 7) and why Ta/U ratios are intermediate between those in MORB and Andean SVZ arc magmas (Fig. 8). Support for a subducted component comes from the observation that the most arc-like ratios occur in the Comallo region plateau lavas (La/Ta = 18–24, Ba/La = 22–32; Th/Ta = 0·37; Ta/U < 2; Figs 7 and 8), which are closest to the SVZ arc front (Fig. 3). The values of these ratios indicate that the amount of subducted component in the Somuncura province lavas is less than in modern SVZ arc (Ba/La ~ 21–28; Sr/La ~ 53–68; Th/La ~ 0·15–0·30; La/Ta ~ 40–75; Th/Ta ~ 8–21) and back-arc (Ba/La ~ 15; Sr/La ~ 17; Th/La ~ 0·18; La/Ta ~ 18; Th/Ta ~ 5) lavas.

The OIB and MORB-like trace element ratios in Eocene and pre-plateau Ranquil Huao lavas (Ba/La < 18; La/Ta < 14; Th/Ta < 2; Ta/U > 2·2; Figs 7 and 8) show no evidence of a subduction-like component. Entry of this component is signaled by the transitional arc-like low Ta/U (down to 1·4; Fig. 8) and high Ba/La (14–38) and Sr/La (25–70) (Fig. 7) in the plateau lavas. The presence of transitional arc-like ratios in some of the eastern and central plateau lavas shows that the effect of this component was not limited to the western Somuncura province. Particularly notable are ratios of La/Ta up to 19, Ba/La up to 38 and Sr/La up to 70 in early and main plateau lavas from the northeastern part of the Meseta de Somuncura and in the Coña Niyeu sequence (Fig. 7). A comparison of lavas within sequences and across the region shows that the arc-like affinities in terms of Ba/Ta, Ba/La, Sr/Ta, Sr/La, Th/Ta and Th/La increase from the pre-27 Ma pre-plateau Ranquil Huao lavas to the ~27 Ma plateau lavas near the top of the Ranquil Huao sequence to the <26 Ma northeastern plateau and Coña Niyeu lavas (Figs 7 and 8). This pattern changes in the uppermost plateau and post-plateau lavas, which continue to have high Ba/Ta ratios but show a reversal to lower Sr/Ta, Sr/La, Th/La and Ta/U ratios (Figs 7 and 8).

The easiest way to explain entry of a subducted component into the magma source at the time of plateau magmatism is for a subducting slab and/or slab-modified mantle to dehydrate and trigger the melting event that produced the plateau magmas. Notably, the enrichments in fluid-mobile elements (Sr, Ba, and U) were accompanied by little to no arc-like depletion of the HFSE as evidenced by the lack of negative Ta anomalies in extended trace element plots in Fig. 5 and the restricted range of MORB- or OIB-like La/Ta ratios (most 10–15) in the majority of the plateau and post-plateau lavas (Fig. 7). One explanation is that the

thermal processes that produced the plateau magmas destabilized oxide phases that formed either in or above the subducting slab (e.g. Reagan & Gill, 1989) releasing incorporated Ti and HFSE. Subduction zone models that attribute HFSE depletion to differential element mobility in fluids (e.g. see Elliot *et al.*, 1997) provide no easy explanation as to why Ta was not depleted as Ba, Sr and U were enriched in the magma source.

Increases in Th/Ta and Th/La ratios, which accompany those in Ba/La and Sr/La in the plateau lavas, require addition of Th as well as Ba and Sr to the magma source (Figs 7 and 8). As Th is generally immobile in fluids, Th enrichment in arc magmas is commonly linked to melting of subducted sediment (see review by Elliot *et al.*, 1997) or incorporation of crust into the mantle wedge by forearc subduction erosion (e.g. Stern, 1991; Kay *et al.*, 2005). Both processes could play a role in the petrogenesis of the plateau lavas. Removal of the forearc margin by subduction erosion during the Oligocene oblique convergence regime, or as the plate margin adjusted to changes associated with the breakup of the Farallón plate, could explain why: (1) Th/Ta ratios are higher in some plateau than in post-plateau lavas; (2) $^{87}Sr/^{86}Sr$ ratios are higher and εNd values lower in plateau lavas at Comallo (0·7050–0·7051; εNd ∼ –2) than in late Oligocene lavas to the west (0·7035–0·704; εNd ∼ +3·3 to +5) (Fig. 9; Table 7).

Another issue is why Ba/La ratios remain high in the post-plateau lavas, whereas Sr/La (<30), Th/La, La/Ta (<16), and Ta/U ratios are close to pre-plateau levels (Figs 7 and 8). Lower Sr/La ratios are not attributable to plagioclase fractionation, as post-plateau lavas generally have higher Sr contents and can have positive Eu anomalies (Eu/Eu* up to 1·2). Relative decreases in ratios involving Sr, Ba, and Th are better explained by a depletion of subducted components in the magma source. The relatively high Ba/Ta and Ba/La ratios could be due to phlogopite formation in the lithospheric mantle during the plateau stage, consistent with the eruption of the high-K orendite suite near 20 Ma (Corbella, 1982*c*).

Mantle source components, melting percentages and depths of melting

The dominant component by volume in the Somuncura province magmas comes from the mantle. Unraveling the origin of the mantle-derived magma requires constraining the mantle source composition and the depth and temperature of melting. Much can be learned by analogies with oceanic intra-plate lavas, particularly the well-studied ones in Hawaii. A number of similarities are notable. (1) The LREE to HFSE ratio as measured by La/Ta ratios ranges from ∼10 to 16 in both oceanic intra-plate (e.g. Hickey *et al.*, 1986; Huang & Frey, 2003) and most Somuncura lavas (Fig. 7). (2) Somuncura province lavas show the Hawaiian Haleakala-like pattern of low and high LILE concentrations combined respectively with more and less enriched Sr–Nd isotopic signatures (Figs 5 and 9) that was made famous by Chen & Frey (1985). Specifically, the plateau lavas are like Hawaiian shield and post-shield lavas in being characterized by low Th, Ba, Sr, and LREE concentrations and $^{143}Nd/^{144}Nd$ ratios along with high Ba/La, Th/La, and $^{87}Sr/^{86}Sr$ ratios, whereas the pre- and post-plateau lavas are like Hawaiian pre-shield and post erosional lavas in showing the opposite pattern of high and low values. (3) The shapes of Somuncura pre-plateau, plateau and post-plateau REE patterns are reminiscent of those of Hawaiian pre-shield, late main shield, and post-erosional lavas. The nearly flat LREEand steep HREE patterns in some of the plateau lavas (Fig. 5) are rare in continental and most oceanic island lavas (Fig. 6; review by Lassiter & DePaolo, 1997), but common in Hawaiian shield-forming flows (e.g. Feigenson *et al.*, 1996; Yang *et al.*, 1996). Understanding the origin of these patterns has been a longstanding problem in Hawaiian magmatism (e.g. Feigenson *et al.*, 1996).

Trace element models provide constraints on mantle melting percentages and source compositions for the Somuncura magmas. Relative melting percentages can be estimated from Fig. 12, which shows Th concentrations (ppm) vs chondrite-normalized La/Sm ratios for Somuncura flows with >250 ppm Cr compared with calculated melting curves from Gorring & Kay (2001). Melting percentages inferred by comparisons with these model curves are minima as differentiation and AFC processes increase both Th contents and La/Sm ratios. The mantle sources in the Gorring & Kay (2001) models (described in the caption of Fig. 12) were chosen for Patagonian back-arc lavas in the Triple Junction province (Fig. 1). These models can be applied to the Somuncura lavas. An 'enriched source' (0·885 ppm La; 0·414 ppm Sm; 0·113 ppm Th) is needed to approximate the characteristics of the late plateau, pre-plateau and post-plateau lavas. A less enriched source (0·481 ppm La; 0·380 ppm Sm; 0·600 ppm Th), which is a mixture of 50% of a MORB-type source with a mantle source whose trace element concentrations are two times the Leedy chondrite (Masuda *et al.*, 1973), is needed to explain the lower Th contents at a given La/Sm ratio in the early and main plateau lavas, and to keep their melting percentages at realistic values.

The calculated melting models indicate higher relative partial melting percentages for the voluminous plateau lavas than for the less voluminous pre- and post-plateau lavas. The most depleted sources and nearly the highest melting percentages (∼10%) are inferred for the Comallo lavas (Fig. 12) that occur just east of the Paleogene arc. Their relatively high Ba/La and La/Ta

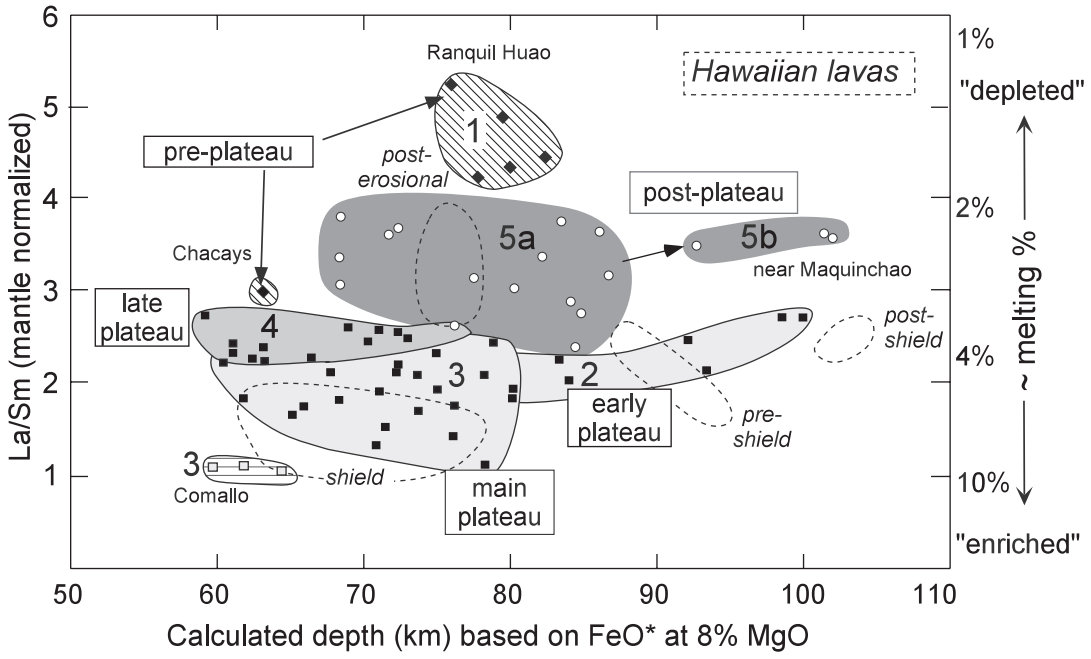

Fig. 13. Calculated depth of magma segregation inferred from measured FeO* (total Fe as FeO) projected to 8% MgO vs primitive mantle normalized La/Sm (La = 0·687 ppm, Sm = 0·444 ppm; Sun & McDonough, 1989) and relative melting percentage inferred from Fig. 12. Calculated depth is based on linear regressions of FeO* in the experiments of Hirose & Kushiro (1993) on Hawaiian lherzolite HK-66. Equations are from Scarrow & Cox (1995): pressure (GPa) = [–25·56 + 4·35 × FeO^{total} (wt %)]/10; depth (km) = 30·2 × P (GPa) + 5. Samples with the shallowest calculated depths have the highest inferred melting percentages and the lowest FeO* concentrations. Fields for Hawaiian pre-shield, shield, post-shield, and post-erosional flows (dashed fields) are based on analyses by Watson (1993). Numbers in fields show the temporal sequence inferred for the Somuncura province pre-plateau (1), plateau (early—2; main—3; late—4) and post-plateau stages (5a and 5b). (See discussion in text.)

ratios (Fig. 7) are consistent with a hydrous slab-derived component enhancing melting of a relatively depleted source. Most early and main plateau lavas, like most Hawaiian lavas, plot between the curves for the more and less enriched sources in Fig. 12. Melting percentages are variable, with the highest percentage melts (>10%) corresponding to the long flows in the northeastern region and to Coña Niyeu region flows (Fig. 3). The late plateau flows plot along or above the curve for the enriched source and have inferred melting percentages from ~4 to 7%. The modeling implies ~2·5–3% partial melting of an enriched source for the post-plateau flows and <2·5% partial melting for the pre-plateau Ranquil Huao flows.

Melting depths for the Somuncura magmas can be estimated by looking at their major element compositions relative to those of experimental melts (e.g. Langmuir *et al.*, 1992; Scarrow & Cox, 1995; Turner & Hawkesworth, 1995). Some relevant experiments are on Hawaiian lherzolite HK66 (Hirose & Kushiro, 1993). The premise for determining depth of melting is that FeO* (total Fe as FeO) contents in magmas derived from similar sources are strongly dependent on pressure and nearly independent of melting percentage. Calculated depths for the Somuncura flows in Fig. 13 are for FeO* contents that have been corrected to 8% MgO by numerically adjusting phenocryst percentages or graphical projection. Measured MgO contents range from 9 to 4% (Tables 3–5). Uncertainties in the extrapolations and the assumption of a common source make relative depths more meaningful than calculated depths. Lower MgO contents in pre- and post-plateau lavas than in the plateau lavas at a given FeO* result in shallower calculated melting depths for the plateau lavas. Following Langmuir *et al.* (1992), the calculated depths are average segregation depths of pooled magmas and are proportional to the range of depths over which melting occurred or the length of the melting column. Given a constant mantle potential temperature or T_p (temperature after adiabatic rise to surface assuming no melting or phase change), shallower depths imply incremental melting over a longer melting column, whereas greater depths imply shorter melting columns and conditions approaching batch melting. Greater melting depths generally translate into a thicker lithosphere.

Other constraints on depth of melting come from garnet-free or garnet-bearing residual mineral assemblages inferred from trace element data. Garnet is important in constraining mantle potential temperature as it is unstable above ~60 km in an anhydrous mantle with a T_p of ~1300°C and above ~80 km in a plume-like mantle with a T_p of ~1500°C (e.g. McKenzie &

O'Nions, 1991). A longstanding problem in Hawaiian magma genesis has been that experimental studies on Hawaiian peridotites (e.g. KLB-1; Herzberg & Zhang, 1996) indicate that garnet should be present in the mantle source for lavas with steep HREE patterns, whereas models for the LREE indicate that garnet should be melted out within a high-temperature plume-like mantle. Based on models for Hawaiian magmas, the flat LREE and steep HREE chondrite-normalized patterns (Figs 5 and 6) of the Somuncura plateau lavas can be explained either by batch melting of a garnet-bearing mantle source with a flat REE pattern, or by incremental or batch melting of a garnet-free source with a flat LREE and steep HREE pattern (see Feigenson *et al.*, 1996).

An interesting pattern emerges when FeO*-based depths (Fig. 13) are compared with inferred mantle melting percentages (Fig. 12) and Nd–Sr isotopic ratios (Fig. 9). Fields representing five stages are shown in Fig. 13 along with comparative fields for some Hawaiian shield, post-shield and post-erosional magmas. Like Hawaiian magmas, the Somuncura magmas show a temporal trend from relatively 'depleted' (pre-plateau) to 'enriched' (plateau) to 'depleted' (post-plateau) isotopic signatures as melting percentages increase and depths first decrease and then reverse (Figs 9 and 13). Lassiter *et al.* (1996) interpreted the Hawaiian trend as reflecting variable melting conditions as the magmas developed over a migrating plume source. In the Hawaiian model, pre-shield melts develop over the approaching plume, shield and post-shield magmas form in the main part of the plume, and post-erosional magmas reflect incorporation of lithospheric sources into the departing plume. With some caveats, Somuncura stages 2–5 have parallels with Hawaiian pre-shield to post-erosional chemical and isotopic trends.

Another aspect of the Somuncura province lavas is the comparability of their isotopic ratios to those of mantle plume-related basalts. As seen in Figs 9 and 10, Sr–Nd–Pb isotopic ratios in Somuncura province lavas generally fall between those of Hawaiian-type and southern Atlantic Tristan da Cunha- and Walvis Ridge-type plume sources. Somuncura lava $^{87}Sr/^{86}Sr$, $^{143}Nd/^{144}Nd$, and $^{206}Pb/^{204}Pb$ are closer to the Atlantic-type sources and are similar to those of Etendeka Tafelkop lavas described by Ewart *et al.* (2004). Based on the mixing lines that Ewart *et al.* (2004) used to model the Etendeka lavas, the $^{87}Sr/^{86}Sr$, $^{143}Nd/^{144}Nd$, $^{208}Pb/^{204}Pb$, and $^{206}Pb/^{204}Pb$ of the Somuncura lavas can be described as mixtures of ~60% of a Tristan da Cunha-type mantle source component and ~40% depleted mantle (DM) along with a minor amount of subducted sediment. The Somuncura data support a greater proportion of a Tristan da Cunha-like mantle source component in the plateau lavas than in the pre- or post-plateau lavas. Such a model is in accord with the higher $^{87}Sr/^{86}Sr$ ratios of the plateau lavas, reflecting asthenospheric mantle as well as crustal sources, and reduces the amount of crustal contaminant needed to explain their isotopic ratios. Elevated $^{207}Pb/^{204}Pb$ ratios in the Somuncura magmas require some contribution from old continental crust that is either from subducted sediment or within the crust. Overall, the Somuncura data support mixing of a Tristan da Cunha-type plume source and ambient DM with minor amounts of subducted and *in situ* continental crust (Figs 10 and 14).

EVOLUTION OF THE SOMUNCURA PROVINCE: A MAGMATIC–TECTONIC MODEL FOR INTERACTION OF A PLUME-LIKE UPWELLING AND A SUBDUCTING PLATE

Parallels between Somuncura and Hawaiian magma evolution, along with the lack of any other explanation, led Kay *et al.* (1992, 1993) to suggest that a transient mantle thermal anomaly related to changes in plate convergence vectors caused the Somuncura province to form. Subsequently, Muñoz *et al.* (2000) argued that Oligocene to early Miocene magmas from the Meseta de Somuncura to the Chilean coast formed in an asthenospheric upwelling through a slab window, created by slab rollback as the shallowly dipping Farallón plate evolved into a steeply dipping Nazca plate. In contrast, de Ignacio *et al.* (2001) speculated that the thermal anomaly was caused by a shallow asthenospheric upwelling induced and focused into the Somuncura region by a concave-up slab geometry. Both models are predicated on assumed slab geometries. The new three-stage model shown in Fig. 14 and discussed below takes into account all of the available geochemical and geological data. The model calls for a mantle upwelling to intersect a relatively steeply subducting Farallón plate. As before, the upwelling is linked to a mantle disturbance as plate convergence vectors changed to the west. Another factor could be a near-stable position of the South American plate relative to the hotspot reference frame. Melting is argued to be localized by a mantle wetspot that formed in relation to a Paleogene volcanic arc.

Stage 1: pre-plateau volcanism in an oblique convergence regime (Fig. 14a)

The initiation of the Somuncura province is marked by the eruption of intraplate-like late Oligocene pre-plateau mafic and silicic magmas. In accord with their chemistry,

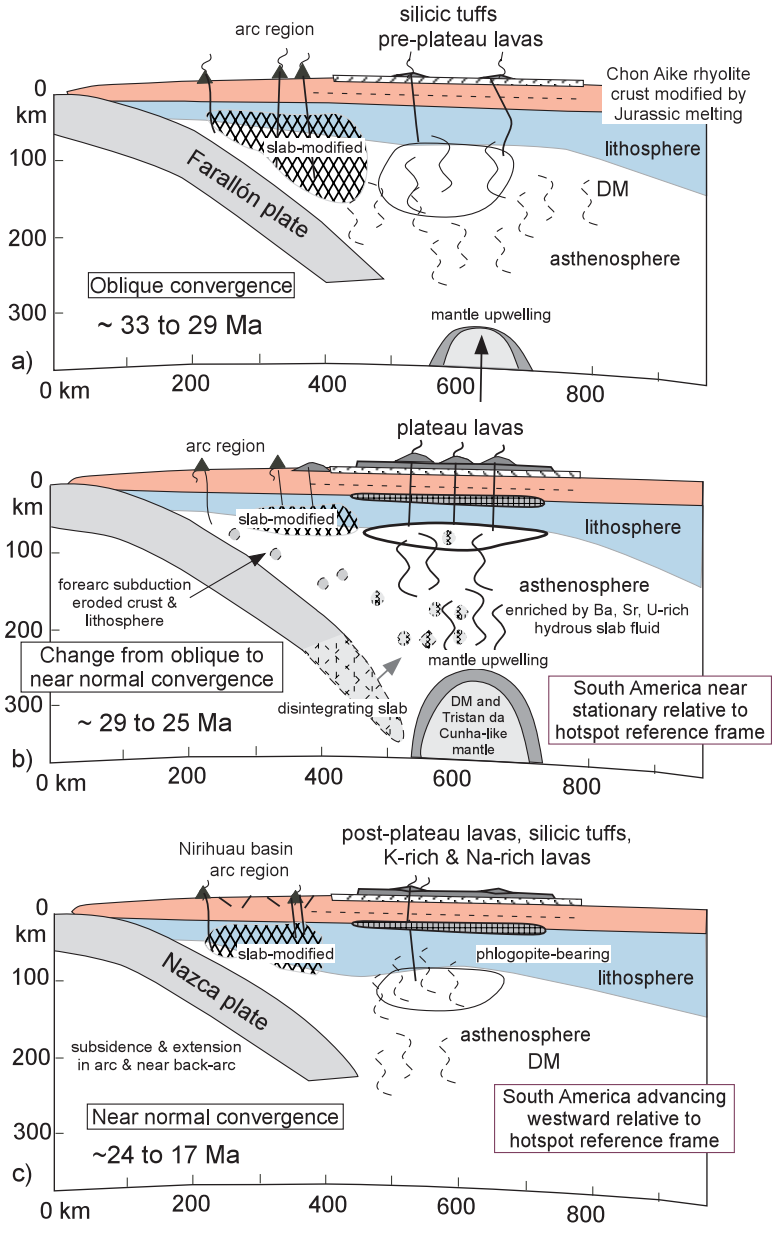

Fig. 14. Schematic illustration of the three-stage evolutionary model for the Oligocene to early Miocene Somuncura province pre-plateau, plateau and post-plateau volcanic rocks. In the model, magmatism is triggered by an asthenospheric mantle upwelling that formed during a period of mantle instability at a time of oceanic plate reorganization. The upwelling intersects the subducting Farallón plate. Melting is facilitated by mantle hydration related to Paleogene subduction, and possibly by heating as a result of the South American plate being nearly stationary relative to the underlying mantle during this period. (See text for discussion.) (a) In the pre-plateau stage from ~32 to 29 Ma, small-percentage mantle melts rise above the upwelling mantle in the back-arc region as extension accompanies oblique subduction in the arc region. The back-arc lavas erupt east of the influence of the subducted plate. (b) In the plateau stage from ~29 to 25 Ma, mantle upwelling accelerates magma generation in the back-arc asthenosphere and a magmatic lull appears to occur in the arc. The mantle melts incorporate subducted components and hydrated mantle from above and within the remnant Farallón plate. The relatively dense Fe-rich mantle-derived magmas pond near the base of the crust, where they fractionate until they are light enough to rise. Intermediate to silicic magmas originate in the crust by melting of underplated mafic magmas, fractionation, assimilation of crustal rocks and mixing. Plateau lavas across the region show a hydrous subduction imprint, little to no arc-like HFSE depletion and little effect from the continental crust, which lost most of its low-temperature melting fraction during the Jurassic. An arc chemical signature in strongest in the westernmost plateau lavas. (c) In the last stage from ~24 to 17 Ma, low-percentage mantle melts associated with ebbing of the upwelling and thickening and of the cooling lithosphere produce the post-plateau lavas. Depletion of hydrous components leads to CO_2 becoming a more important volatile phase in the mantle. Late-stage melting of enriched lithosphere produces high-K and high-Na lavas. Arc volcanism resumes in the early Miocene in response to fast orthogonal subduction of the Nazca plate (e.g. Somoza, 1998). Slab roll-back produces extension and thermal subsidence leading to marine ingression from the east and the development of the Nirihuau basin (Cazau *et al.*, 1987). Extension largely wanes by 18 Ma (Kay & Copeland, 2006); Somuncura post-plateau volcanism lasts until ~17 Ma.

these magmas are shown in Fig. 14a as erupting over an incipient plume-like mantle upwelling, east of any influence of a steeply subducting slab in an oblique convergence regime. Support for the pre-plateau flows being small-percentage melts of a relatively isotopically 'depleted' garnet-bearing mantle source comes from their trace element and isotopic signatures (Figs 7–10). Like the Eocene flows before them, their intraplate-like trace element characteristics and 'depleted' Nd–Sr isotopic ratios show little effect of crustal or slab-related components. Their FeO*-based depths of melting are consistent with batch melting below an ~80–90 km thick continental lithosphere (field 1 in Fig. 13). Flows to the west with variable arc-like trace element signatures (La/Ta = 16–38) and relatively low $^{87}Sr/^{86}Sr$ ratios and high εNd (> +1·8) values (Figs 8 and 9; Kay & Rapela, 1987; Kay *et al.* 1993; Muñoz *et al.*, 2000) are shown in Fig. 14a to be located over a region of slab-modified mantle affected by the oblique convergence regime between the Farallón and South American plates (Cande & Leslie, 1986; Somoza, 1998).

Stage 2: plateau volcanism in a changing convergence region (Fig. 14b)

The main development of the Somuncura province is marked by the eruption of the plateau lavas. The model in Fig. 14b explains their principal features by invoking a disintegrating subducting slab, a plume-like mantle upwelling, a thinning mantle lithosphere, ponding of magmas at the base of the crust before eruption, and fractionation and mixing of new melt batches with partially melted underplated magmas to produce the silicic magmas.

A key aspect of the model is the disintegration of the subducting slab at the time of the plume-like mantle upwelling. The release of subducted components helps to explain the higher Sr, Ba, U, and Th to LREE ratios, higher $^{87}Sr/^{86}Sr$ ratios, and lower εNd values in the plateau compared with the pre-plateau lavas. The model differs from that of Muñoz *et al.* (2000), who attributed the arc-like ratios in the Somuncura province magmas to components introduced into the lithosphere over a relatively shallow Paleogene subduction zone. The problem with their model is how to introduce subducted components into the lithosphere up to 800 km east of the modern trench between the eruption of the pre-plateau and the plateau lavas. A flat-slab geometry seems improbable given the short time, the obliquity of Paleogene convergence, and the lack of deformational or magmatic evidence for a Paleogene or late Mesozoic flat-slab geometry (e.g. Kay & Abbruzzi, 1996; James & Sacks, 1999). A slab disintegration model like that called upon by Stern *et al.* (1990) to explain the presence of arc-like components in Plio-Pleistocene back-arc lavas is better. Such a model works well for the Somuncura province magmas as a plume-like mantle upwelling can accentuate slab disruption and could facilitate the dispersion of subducted components far to the east. An association of arc-like fluid-mobile element signatures (high Ba/La and Sr/La) with weak to absent arc-like HFSE depletions (low La/Ta ratios) in the plateau lavas (Fig. 7) fits with HFSE-bearing oxide phases being destabilized as a result of the breakdown of the slab and the oxidizing environment that produced them (e.g. Reagan & Gill, 1989). Enrichments in Th can be attributed to melting of subducted sediment or crust removed by fore-arc subduction erosion as the plate margin adjusted to changing convergence vectors.

The other key feature of the model is the plume-like mantle upwelling, which explains the voluminous and widespread plateau lavas as decompression-induced melts of mixtures of DM and EM1-like Tristan de Cunha-type mantle (Figs 9 and 10). The changing chemical characteristics and inferred FeO*-based melting depths in the early, main and late-stage plateau lavas (fields 2–4 in Fig. 13) can be reconciled with a lengthening melting column below a thinning mantle lithosphere.

The early plateau stage is exemplified by the <29 Ma to 27 Ma Ranquil Huao flows erupted from the Apas–Chacays region center. Their chemistry can be interpreted as recording an increasing temperature as the plume-like upwelling intensified mantle melting. Evidence comes from La/Sm ratios and Th contents indicating higher partial melting percentages (~6–8%) of a more enriched mantle (Fig. 12) at FeO*-calculated depths ranging from ~100 km at the base to 80 km at the top of the sequence (field 2; Fig. 13). Higher $^{87}Sr/^{86}Sr$ ratios and lower εNd values (Fig. 9) than in the pre-plateau lavas fit with an increased contribution from a Tristan da Cunha-like plume source. High Ba/La, Sr/La and Th/La ratios (Figs 7 and 8) signal the entry of subducted components into the mantle source. Higher $^{207}Pb/^{204}Pb$ isotopic ratios (Fig. 10) require an additional old crustal contaminant.

The main plateau stage at the peak of melt production is exemplified by the large-volume ~27–25 Ma flows from the Alta de Somuncura region center(s) in the east and the Comallo region flows in the west. A peak of melting coincident with the eastern flows is consistent with an increased melting percentage inferred from Th contents and La/Sm ratios (~9–12% for Coña Niyeu and NE flows; Fig. 12). These flows have the highest $^{87}Sr/^{86}Sr$ and lowest εNd in the eastern region (Fig. 9), in accord with a hotter and deeper mantle source influenced by a Tristan da Cunha-like (EM1) mantle plume. Their FeO*-based melting depths of 80–60 km are consistent with a lengthening melt column and a peak in lithospheric thinning. The formation of the Comallo lavas to the west could also

coincide with the peak of the thermal event. Their chemistry fits with a high partial melting percentage (>10%) of an LREE-depleted source (Fig. 12) at a shallow Fe*-based depth (<65 km, Fig. 13). Their LREE-depleted characteristics, transitional arc-like Ba/La (24–31), Sr/La and La/Ta (16–23) ratios, high $^{87}Sr/^{86}Sr$ ratios, and low εNd values are consistent with a depleted lithosphere source component enriched by hydrous subducted components. A plume-like asthenospheric component provides an explanation for a more 'enriched' isotopic signature than in the Ventana Formation arc lavas to the west (Table 6; Figs 2b and 9).

The late-plateau stage flows erupted across the region at ~26–24 Ma. As seen in the upper flows at Coña Niyeu, these lavas have higher Th contents and lower La/Sm ratios that result in lower calculated partial melting percentages (~6–3%; Fig. 12), providing evidence for the passing of the main thermal peak. Lower $^{87}Sr/^{86}Sr$ ratios and higher εNd values in the late plateau upper Coña Niyeu and Valcheta region flows (Fig. 9) can be interpreted as recording a return to an increased role for depleted lithospheric source components. FeO*-based depths of 80–60 km are consistent with the residual effects of a long melting column and a continued thin lithosphere (field 4, Fig. 13).

The final feature of the model is the ponding of the plateau magmas near or at the base of the crust prior to eruption, in accord with evidence for olivine and pyroxene fractionation (low Mg, Ni, and Cr contents) at the expense of plagioclase (small Eu anomalies) and non-primitive compositions. In this setting, silicic trachytic and rhyolitic magmas can form by partial melting of previously underplated magmas. Fractionation of mafic magmas and mixing with silicic melts can produce benmoreite and trachytic magmas. The Sr–Nd–Pb isotopic similarities between the mafic and silicic magmas (Figs 9 and 10) indicate that little pre-existing crust was incorporated, in accord with a refractory crust that had lost most of its low-temperature melting component in the formation of the Jurassic Chon Aike rhyolites.

Stage 3: post-plateau magmatism in a near-normal convergence regime (Fig. 14c)

The last stage of the Somuncura province volcanism is marked by eruption of the ~24–17 Ma post-plateau lavas in a band from the Carri Laufquen to the Telsen region (Fig. 3). The origin of these lavas must be considered in the context of the Somuncura province, as well as the widespread Patagonian volcanism and evidence for extension to the west at this time (e.g. Cazau *et al.*, 1987; Muñoz *et al.*, 2000; Jordan *et al.*, 2001; Kay and Copeland, 2006; Fig. 1).

The model in Fig. 14c explains the chemistry of the post-plateau lavas relative to the ebbing of a plume-like upwelling. Decreased mantle melting is signaled by steeper HREE patterns (Figs 5e and 6) and trace element evidence for lower partial melting percentages (2·5–3%; Fig. 12) of a garnet-bearing mantle. A general return to FeO*-based depths of ~70–85 km (field 5a, Fig. 14) is consistent with shortening of the melting column under a cooling lithosphere. The persistence of high Ba/La ratios can be explained by breakdown of sequestered phlogopite in the lithospheric mantle. An ~5 Ma lapse between plateau and post-plateau magmatism in some places resembles that east of the Chile Triple Junction (Fig. 1), which Gorring *et al.* (1997) attributed to decompression melting of a more CO_2-enriched asthenosphere at the ebb of the thermal event. The relative increase in CO_2 in the mantle would be expected in association with a return to more alkaline magmas (e.g. Hirose, 1997) with OIB- and MORB-like Sr/La, Sr/Ta and Ta/U ratios (Figs 7 and 8). In this context, the ~20 Ma lavas near Maquinchao are distinctive for their lower $^{87}Sr/^{86}Sr$ ratios and higher εNd values (Fig. 9), and Fe*-based depths of ~90–100 km (field 5b in Fig. 13). Their relatively high Th contents and La/Sm ratios suggest low partial melting percentages (<3%). At the same time, the ~17 Ma flows near Telsen have Nd–Sr isotopic compossitions (Fig. 9) and trace element-based melting percentages similar to those of the late plateau flows (Fig. 12). One explanation for this contrast is that the mantle under the Maquinchao region was cooled by the nearly orthogonally subducting Nazca plate, whereas higher temperatures persisted east of the influence of the subducting plate in the mantle under the Telsen region.

The post-plateau flows are also temporally associated with Na-rich volcanic rocks on and north of the Meseta de Somuncura and high-K volcanic rocks to the south. The restriction of Na- and K-rich volcanic rocks to this part of Patagonia at this time points to a continued distinctive mantle history under the Somuncura region. The best explanation for these volcanic rocks is that they are largely low-percentage partial melts of a phlogopite- and amphibole-rich lithosphere. The presence of these hydrous phases in the lithosphere can be linked to the residual effects of dehydration of the disintegrating slab and mantle melting related to the plume-like mantle upwelling.

Why is there a hotspot-like mantle upwelling in the Somuncura region?

The late Oligocene to early Miocene Somuncura province is one of a series of Late Cretaceous to Recent magmatic provinces in Patagonia that show no pattern in space and time and cannot be related to a known hotspot (Fig. 1). On a global scale, the topographic expression of the Meseta de Somuncura is comparable with that of African plateaux such as Tibesti and

Hoggar, which Burke & Wilson (1972) attributed to hotspots without trails as they occur on a stationary plate in a global hotspot reference frame. Such a model does not easily explain the Patagonian provinces on the more mobile South American plate. Nevertheless, there are similarities between the Somuncura and Cenozoic African centers. Like the Somuncura province, many of the African centers lie outside the boundaries of Cretaceous rift zones, are associated with broad basement uplifts, and have no obvious link to extension. Based on these characteristics and others, Wilson & Guiraud (1992) suggested that the magmas of the African volcanic centers largely formed from partial melts of basal sub-continental lithosphere that had been metasomatized by Mesozoic–Cenozoic plume activity. A similar model for the Somuncura magmas is difficult to reconcile with temporal changes in the erupted lavas. However, a common feature could be a nearly stable position of South America relative to the hotspot reference frame at the time. Additional support comes from Silver *et al.* (1998), who argued that a late Oligocene to early Miocene acceleration of the South America plate relative to the hotspot reference frame led to the uplift of the modern Andes. Kay & Copeland (2006) argued that this acceleration actually began after 20 Ma when post-plateau magmatism was waning in the Somuncura province.

An important question is what triggered the thermal anomaly beneath the Somuncura province. One answer is to relate the anomaly to a mantle instability associated with late Oligocene plate reorganization, as first suggested by Kay *et al.* (1992, 1993). The magmatism could be related to a plume-like upwelling that is hotter than normal mantle and whose existence is justified by global plume heat flux estimates that show that identified plumes account for only ~25% of residual mantle heat flux not explained by subducted slabs (e.g. Davies, 1988*a*, 1988*b*; Sleep, 1990; Turcotte, 1995). Gorring *et al.* (1997) argued for entrainment of such an upwelling in the slab window east of the Chile Triple Junction to explain the large amounts of back-arc volcanism in that region. The Somuncura event has been argued to be one of a series of tectonically induced melting events of a regionally hot Patagonian mantle (Kay *et al.*, 2004).

Another factor in explaining and localizing the Somuncura magmatic province could be hydration of the mantle by the Paleogene subduction zone that produced the arc lavas on the western margin of the Somuncura province (Fig. 1; Rapela *et al.*, 1988; Ardolino *et al.*, 1999). Importantly, Ramos & Kay (1992) pointed out that the Paleogene arc ends near the southern margin of the Somuncura province near ~43°S. They correlated the end of the arc with the northern margin of a slab window(s) created by the collision of the Aluk–Farallón spreading ridge with the Chile trench. A relation with the position of the Paleogene arc could explain the location of the Somuncura province.

CONCLUSIONS

(1) The Somuncura magmatic province constitutes the largest volcanic field in extra-Andean Patagonia. This voluminous magmatism cannot be associated with major extension and has no obvious link to any tectonic event other than late Oligocene plate reorganization to the west. The features of the Somuncura province magmas are best explained by a transient plume-like mantle upwelling that intersected a subducting plate at a mantle 'wetspot'.

(2) Somuncura province volcanic rocks can be generally divided into pre-plateau, plateau and post-plateau groups. Low-volume late Oligocene pre-plateau flows are typically intraplate alkaline basalts and hawaiites with 'depleted' isotopic compositions ($^{87}Sr/^{86}Sr < 0{\cdot}704$; $\varepsilon Nd > +2$). Voluminous ~27 ± 2 Ma plateau flows are dominantly hypersthene-normative basalts and basaltic andesites (50–54% SiO_2) with flat REE patterns (La/Yb = 4–12), relatively low LILE abundances, transitional to arc-like Ba/La, Sr/La, Th/Ta and U/Ta ratios, intraplate La/Ta ratios and 'enriched' Nd–Sr isotopic compositions ($^{87}Sr/^{86}Sr > 0{\cdot}7043$; $\varepsilon Nd < +1{\cdot}3$). Intermediate to low-volume ~23–17 Ma post-plateau flows are dominantly alkali olivine basalts and hawaiites (48–51% SiO_2) with steep REE patterns (La/Yb >15), high LILE abundances, high Ba/La ratios, intraplate Sr/La and U/Ta ratios, and 'depleted' isotopic compositions ($^{87}Sr/^{86}Sr = 0{\cdot}7034$–$0{\cdot}7046$; $\varepsilon Nd = +0{\cdot}9$ to $+4{\cdot}5$).

(3) Support for a relation between the Somuncura province magmas and a plume-like mantle upwelling comes from large-volume plateau flows (>100 km long) whose isotopic compositions can be approximated by mixtures of depleted mantle (DM) and a Tristan de Cunha plume-like mantle source component and whose chemistry has broad parallels with hotspot magmas such as those in Hawaii. These parallels include: (a) Hawaiian tholeiitic-like REE patterns with flat LREE and steep HREE slopes, (b) a similar pattern of FeO*-inferred melting depths, (c) similar partial melting percentages based on Th (ppm) and La/Sm ratios, and (d) a similar pattern of isotopically enriched, LREE- and LILE-poor tholeiitic lavas that erupted before and after isotopically depleted LREE- and LILE-enriched alkaline lavas.

(4) Support for incorporation of subducted components into the Somuncura mantle source associated with a disintegrating slab at the time of the mantle upwelling comes from high Ba, Sr, Th and U to LREE ratios in the plateau lavas. A lack of HFSE depletion in the plateau lavas supports resorption of HFSE-bearing phases

that formed during the subduction process at this time. The subsequent depletion of fluid-mobile elements in the mantle source and sequestering of Ba and K in amphibole and phlogopite in the lithosphere is signaled by high Ba/La and low Sr, Th and U to LREE ratios in the post-plateau lavas and the eruption of high-K orenditic magmas. A return to CO_2 as the more important mantle fluid phase is consistent with the intra-plate-like chemistry in the post-plateau flows.

(5) Evidence for minimal crustal contamination in the Somuncura plateau magmas comes from low LILE (Sr) and REE (Nd) abundances coupled with radiogenic isotopic compositions whose changing character can be largely explained by processes in the mantle. Limited crustal contamination is consistent with a crust whose low melting fraction was extensively depleted by massive crustal melting in the Mesozoic.

(6) Silicic Somuncura province magmas including trachytes, phonolites and rhyolites can be attributed to crystal fractionation, partial melting of underplated Somuncura type mafic magmas and mixing of these melts with mafic magmas.

(7) Generation of a late Oligocene plume-like mantle anomaly in the Somuncura region is best attributed to a local mantle thermal instability at the time of plate reorganization, possibly in combination with a nearly stable position of South America relative to the hotspot reference frame. Extensive mantle melting was aided by hydration of the mantle during Paleogene subduction in the Somuncura region.

ACKNOWLEDGEMENTS

We thank C. W. Rapela, M. Franchi and R. W. Kay for discussion and participation in various aspects of the field work; D. L. Turcotte, W. M. White, B. Coira, and H. Corbella for discussion; J. A. Cortés for Eocene samples from the Meseta del Canquel region; and P. Ziegler for facilities for Ar/Ar dating at Lehigh University. The manuscript benefited from reviews by Marjorie Wilson, Julian Pearce, Charles Stern, and an anonymous reviewer. This research was funded in part by the US NSF (EAR-8803732, EAR-9219328 and EAR-0087515), the Argentine Geologic Survey (SEGEMAR), and an American Republics Fulbright fellowship to Kay.

SUPPLEMENTARY DATA

Supplementary data are available at *Journal of Petrology* online.

REFERENCES

Ardolino, A. (1987). Descripción geológica de la hoja 43f, Sierra de Apas, provincia del Chubut. *Dirección Nacional de Minería and Geología* **203**, 1–91.

Ardolino, A. & Franchi, M. (1993). El vulcanismo Cenozoico de la Meseta Somún Curá, Río Negro y Chubut. *XII Congreso Geológico Argentino Actas* **4**, 225–235.

Ardolino, A., Franchi, M., Remesal, M. & Salini, F. (1999). El volcanismo en la Patagonia extrandina. In: Caminos, R. (ed.) *Geología Argentina. Servicio Geológico Nacional Anales* **29**, 579–612.

Bjerg, E. A., Nfatlos, T., Kurat, G., Dobosi, G. & Labudia, C. (2005). The upper mantle beneath Patagonia, Argentina, documented by xenoliths from alkali basalts. *Journal of South American Earth Sciences* **18**, 125–145.

Bohrson, W. A. & Spera, F. J. (2001). Energy-constrained open-system magma processes II: Application of energy-constrained assimilation–fractional crystallization (EC-AFC) model to magmatic systems. *Journal of Petrology* **42**, 1019–1041.

Burke, K. & Wilson, J. T. (1972). Is the Africa plate stationary? *Nature* **239**, 387–390.

Cande, S. C. & Leslie, R. B. (1986). Late Cenozoic tectonics of the southern Chile Trench. *Journal of Geophysical Research* **91**, 471–496.

Cazau, L., Mancini, C., Cangini, J. & Spalletti, L. (1987). Cuenca de Nirihuau. In: Chebli, G. & Spalletti, L. (eds) *Cuencas Sedimentarias de Argentina. Serie Correlación Geológica, Universita Nacional de Tucumán*, **6**, 299–318.

Chen, C.-Y. & Frey, F. A. (1985). Trace element and isotopic geochemistry of lavas from Haleakla Volcano, East Maui, Hawaii: implications for the origin of Hawaiian basalts. *Journal of Geophysical Research* **90**, 8743–8768.

Coffin, M. F. & Eldholm, O. (1994). Large igneous provinces—crustal structure, dimensions and external consequences. *Reviews of Geophysics* **32**, 1–36.

Coira, B., Franchi, M. & Nullo, F. E. (1985). Vulcanismo terciario al oeste de Somuncurá y su relación con el arco magmático de la Cordillera Nordpatagónica, Argentina. *IV Congreso Geológico Chileno Actas* **4**, 68–88.

Corbella, H. (1982a). Complejo volcánico alcalino Sierra de Telsen, Patagonia extraandina, Argentina. *V Congreso Latinoamericano de Geología Actas* **2**, 225–238.

Corbella, H. (1982b). Quimismo del complejo volcánico alcalino Sierra Negra de Telsen, Patagonia extrandina norte, Argentina. 1 Elementos mayores. *Asociación Argentina de Mineralogía, Petrología y Sedimentología Revista* **13**, 29–38.

Corbella, H. (1982c). Naturaleza litológica del complejo alcalino Sierra de Queupuniyeu, Patagonia extrandina norte, Argentina. *V Congreso Latinoamericano de Geología Actas* **2**, 197–211.

Corbella, H. (1983). Hallazgo de rocas leuciticas perpotasicas en la Sierra de Los Chacays, Patagonia extrandina, Provincia de Chubut. *Asociación Argentina de Mineralogía, Petrología y Sedimentología Revista* **14**, 88–96.

Corbella, H. (1984). El volcanismo de la Altiplanicie del Somuncurá. In: Ramos, V. (ed.) *Geología y Recursos Naturales de la Provincia de Rió Negro. IX Congreso Geológico Argentino Relatorio*, pp. 267–300.

Corbella, H. (1985). Foiditas noseánicas y otras volcanitas básicas en la Alta Sierra del Somuncurá, Patagonia extrandina, Argentina. *IV Congreso Geológico Chileno Actas* **4**, 89–107.

Corbella, H. (1989a). Sierra de los Chacays, extrandean Patagonia, Chubut, about the chemistry of the alkaline complex and its potassic and ultrapotassic rocks. *Revista de la Asociación Geológica Argentina* **44**, 96–110.

Corbella, H. (1989b). Sierra de Queupuniyeu, north extrandean Patagonia, Río Negro: the chemistry of the alkaline volcanic units. *Revista de la Asociación Geológica Argentina* **44**, 111–126.

Corbella, H. & Barbieri, M. (1989). Sierra de Chacays, extrandean Patagonia, Chubut, Argentina: $^{87}Sr/^{86}Sr$ isotopic ratios of the alkaline rocks and age of the potassic volcanics of Mt. Plan-Luan. *Revista de la Asociación Geológica Argentina* **44**, 133–140.

Davies, G. F. (1988a). Ocean bathymetry and mantle convection. 1, Large–scale flow and hotspots. *Journal of Geophysical Research* **93**, 10467–10480.

Davies, G. F. (1988b). Ocean bathymetry and mantle convection. 2, Small–scale flow. *Journal of Geophysical Research* **93**, 10481–10488.

de Ignacio, C., López, I., Oyarzún, R. & Márquez, A. (2001). The northern Patagonia Somuncura plateau basalts: a product of slab-induced, shallow asthenospheric upwelling? *Terra Nova* **13**, 117–121.

Elliot, T., Plank, T., Zindler, A., White, W. & Bourdon, B. (1997). Element transport from slab to volcanic front in the Mariana arc. *Journal of Geophysical Research* **102**, 14991–15019.

Ewart, A., Marsh, J. S., Milner, S. C., Duncan, S. C., Kamber, B. S. & Armstrong, R. A. (2004). Petrology and geochemistry of Early Cretaceous bimodal continental flood volcanism of the NW Etendeka, Namibia. Part 1: Introduction, mafic lavas and re-evaluation of mantle source components. *Journal of Petrology* **39**, 191–225.

Feigenson, M. D., Patino, L. C. & Carr, M. J. (1996). Constraints on partial melting imposed by rare earth element concentrations in Mauna Kea basalts. *Journal of Geophysical Research* **101**, 11815–11829.

Gorring, M. L. & Kay, S. M. (2001). Mantle processes and sources of Neogene slab-window magmas in southern Patagonia. *Journal of Petrology* **42**, 1067–1094.

Gorring, M. L., Kay, S. M., Zeitler, P. K., Ramos, V. A., Rubiolo, D. & Fernandez, M. I. (1997). Neogene Patagonian plateau lavas: continental magmas associated with ridge collision at the Chile Triple Junction. *Tectonics* **16**, 1–17.

Hart, S. R. (1984). A large-scale isotope anomaly in the Southern Hemisphere mantle. *Nature* **309**, 753–757.

Herzberg, C. & Zhang, J. (1996). Melting experiments on anhydrous peridotite KLB-1: compositions of magmas in the upper mantle and transition zone. *Journal of Geophysical Research* **101**, 8271–8295.

Hickey, R. L., Frey, F. A., Gerlach, D. C. & Lopez-Escobar, L. (1986). Multiple sources for basaltic arc rocks from the southern volcanic zone of the Andes (34–41°S): trace element and isotopic evidence for contributions from subducted oceanic crust, mantle and continental crust. *Journal of Geophysical Research* **91**, 5963–5983.

Hildreth, W. & Moorbath, S. (1988). Crustal contributions to arc magmatism in the Andes of Central Chile. *Contributions to Mineralogy and Petrology* **98**, 455–489.

Hirose, K. (1997). Partial melt compositions of carbonated peridotite at 3 GPa and role of CO_2 in alkali-basalt magma generation. *Geophysical Research Letters* **24**, 2837–2840.

Hirose, K. & Kushiro, I. (1993). Partial melting of dry peridotite at high pressures: determination of compositions of melts segregated from peridotite using aggregates of diamond. *Earth and Planetary Science Letters* **114**, 477–489.

Huang, S. & Frey, F. A. (2003). Trace element abundances of Mauna Kea basalt from phase 2 of the Hawaii Scientific Drilling Project: petrogenetic implications of correlations with major element content and isotopic ratios. *Geochemistry, Geophysics, Geosystems* **6**, 8711, doi:10.1029/2002GC000322.

James, D. E. & Sacks, I. S. (1999). Cenozoic formation of the Central Andes: a geophysical perspective. In: Skinner, B. (ed.) *Geology and Ore Deposits of the Central Andes. Society of Economic Geology, Special Publication* **7**, 1–25.

Jordan, T. E., Burns, W. M., Veiga, R., Pangaro, F., Copeland, P. & Mpodozis, C. (2001). Mid-Cenozoic intra-arc basins in the Southern Andes. *Tectonics* **20**, 308–324.

Kay, S. M. (2001). Geochemical evidence for a late Miocene shallow subduction zone in the Andean Southern Volcanic Zone near 37°S latitude. *EOS Transactions, American Geophysical Union* **81**, V12C-099.

Kay, S. M. & Abbruzzi, J. M. (1996). Magmatic evidence for Neogene lithospheric evolution of the central Andean 'flat-slab' between 30° and 32°S. *Tectonophysics* **259**, 15–28.

Kay, S. M. & Copeland, P. (2006). Early to middle Miocene back-arc magmas of the Neuquén Basin of the southern Andes: geochemical consequences of slab shallowing and the westward drift of South America. In: Kay, S. M. & Ramos, V. A. (eds) *Evolution of an Andean Margin: a Tectonic and Magmatic Perspective from the Andes to the Neuquén Basin (35°–39° S Lat.). Geological Society of America, Special Papers*, 407, pp. 185–213.

Kay, S. M. & Rapela, C. W. (1987). El volcanismo del Terciario inferior y medio en los Andes Norpatagónicos (40°–42°30′S): origen de los magmas y su relación con variaciones de la oblicuidad de la zona de subducción. *X Congreso Geológico Argentino Actas* **4**, 192–194.

Kay, S. M., Maksaev, V., Mpodozis, C., Moscoso, R. & Nasi, C. (1987). Probing the evolving Andean lithosphere: middle to late Tertiary magmatic rocks in Chile over the modern zone of subhorizontal subduction (29°–31·5°S). *Journal of Geophysical Research* **92**, 6173–6189.

Kay, S. M., Ramos, V. A., Mpodozis, C. & Sruoga, P. (1989). Late Paleozoic to Jurassic silicic magmatism at the Gondwanaland margin: analogy to the Middle Proterozoic in North America? *Geology* **17**, 324–328.

Kay, S. M., Ardolino, A. A., Franchi, M. & Ramos, V. A. (1992). The Somuncura plateau: An Oligo-Miocene 'baby-hotspot' in extra-Andean Patagonia (40·5° to 43°S latitude). *EOS Transactions, American Geophysical Union* **73**, 337.

Kay, S. M., Ardolino, A. A., Franchi, M. & Ramos, V. A. (1993). Origen de la meseta de Somún Curá: distribución and geoquímica de sus rocas volcánicas máficas. *XII Congreso Geológico Argentino Actas* **4**, 236–248.

Kay, S. M., Ramos, V. A. & Gorring, M. L. (2002). Geochemistry of Eocene plateau basalts related to ridge collision in southern Patagonia. *Actas of XV Congreso Geológico Argentina* , contribution 238 (CD-ROM).

Kay, S. M., Gorring, M. L. & Ramos, V. A. (2004). Magmatic sources, setting and causes of Eocene to Recent Patagonian plateau magmatism (36°S to 52°S latitude). *Asociación Geológica Argentina Revista* **59**, 556–568.

Kay, S. M., Godoy, E. & Kurtz, A. (2005). Episodic arc migration, crustal thickening, subduction erosion, and magmatism in the south–central Andes. *Geological Society of America Bulletin* **117**, 67–88.

Kay, S. M., Burns, W. M., Copeland, P. & Mancilla, O. (2006). Upper Cretaceous to Holocene magmatism and evidence for transient shallowing of the Andean subduction zone under the northern Neuquén basin. In: Kay, S. M. & Ramos, V. A. (eds) *Evolution of an Andean Margin: a Tectonic and Magmatic Perspective from the Andes to the Neuquén Basin (35°–39° S Lat.). Geological Society of America, Special Papers*, 407, pp. 19–60.

Klein, E. M. & Karsten, J. L. (1995). Ocean ridge basalts with convergent margin geochemical affinities from the southern Chile Ridge. *Nature* **374**, 52–57.

Langmuir, C. H., Klein, E. M. & Plank, T. (1992). Petrological systematics of mid-ocean ridge basalts: constraints on melt generation beneath ocean ridges. *Geophysical Monograph, American Geophysical Union* **71**, 183–280.

Lassiter, J. C. & DePaolo, D. J. (1997). Plume/lithosphere interactions in the generation of continental and oceanic flood basalts: chemical and isotopic constraints. In: Mahoney, J.J. & Coffin, M. F. (eds) *Large Igneous Provinces: Continental, Oceanic, and Planetary Flood Volcanism. Geophysical Monograph, American Geophysical Union* **100**, 335–356.

Lassiter, J. C., DePaolo, D. J. & Tatsumoto, M. (1996). Isotopic evolution of Mauna Kea volcano: results from the initial phase of the Hawaii Scientific Drilling Projects. *Journal of Geophysical Research* **101**, 11769–11780.

Le Bas, M. J & Streckeisen, A. L. (1991). The IUGS systematics of igneous rocks. *Journal of the Geological Society, London* **148**, 825–833.

Lema, H. A. & Cortés, J. M. (1987). El vulcanismo eoceno del flanco oriental de la Meseta del Canquel, Chubut, Argentina. *X Congreso Geológico Argentino Actas* **4**, 188–191.

Marshall, L. G., Hoffstetter, R. & Pascual, R. (1983). *Geochronology of the continental mammal-bearing Tertiary of South America. Palaeovertebrate, Memoir Extra*, pp 93.

Marshall, L. G., Cifelli, R. L., Drake, R. E. & Curtis, G. H. (1986). Vertebrate paleontology, geology, and geochronology of the Tapera de López and Scarritt Pocket, Chubut province, Argentina. *Journal of Paleontology* **60**, 920–951.

Masuda, A., Nakamura, N. & Tanaka, T. (1973). Fine structure of mutually normalized rare-earth patterns of chondrites. *Geochimica et Cosmochimica Acta* **37**, 239–248.

McKenzie, D. & O'Nions, R. K. (1995). The source regions of ocean island basalts. *Journal of Petrology* **36**, 133–159.

Muñoz, J., Troncoso, R., Duhart, P., Crignola, P., Farmer, L. & Stern, C. R. (2000). The relation of the mid-Tertiary coastal magmatic belt in south–central Chile to the late Oligocene increase in plate convergence rate. *Revista Geológica de Chile* **27**, 177–203.

Orgeira, M. J. & Remesal, M. (1993). Estudio paleomagnético del complejo volcánico de Somún Curá, Argentina. *Revista de la Asociación Geológica Argentina* **48**, 247–264.

Pankhurst, R. J. & Rapela, C. W. (1995). Production of Jurassic rhyolite by anatexis of the lower crust of Patagonia. *Earth and Planetary Science Letters* **134**, 223–236.

Pardo-Casas, F. & Molnar, P. (1987). Relative motion of the Nazca (Farallón) and South American plates since Late Cretaceous time. *Tectonics* **6**, 233–248.

Paslick, C., Halliday, A., James, D. & Dawson, J. B. (1995). Enrichment of the continental lithosphere by OIB melts: isotopic evidence from the volcanic province of northern Tanzania. *Earth and Planetary Science Letters* **130**, 109–126.

Plank, T. & Langmuir, C. H. (1992). Effects of melting regimes on the composition of the oceanic crust. *Journal of Geophysical Research* **97**, 319–329.

Plank, T. & Langmuir, C. H. (1998). The chemical composition of subducting sediment: implications for the crust and mantle. *Chemical Geology* **145**, 325–394.

Ramos, V. A. & Kay, S. M. (1992). Southern Patagonian plateau basalts and deformation: back-arc testimony of ridge collision. *Tectonophysics* **205**, 261–282.

Rapela, C. W. & Kay, S. M. (1988). Late Paleozoic to Recent magmatic evolution of northern Patagonia. *Episodes* **11**, 175–182.

zRapela, C. W. & Pankhurst, R. J. (1993). El volcanismo riólitico del noreste de la Patagonia: un evento meso-jurasico de corta duración origen profundo. *Acts del XII Congreso Geológico Argentino, Mendoza* **4**, 170–188.

Rapela, C. W., Spalletti, L. A., Merodio, J. C. & Aragon, E. (1988). Temporal evolution and spatial variation of lower Tertiary volcanism in the Patagonian Andes (40°–42°30′S). *Journal of South American Earth Sciences* **1**, 75–88.

Reagan, M. K. & Gill, J. B. (1989). Coexisting calc-alkaline and high niobium basalts from Turrialba Volcano, Costa Rica: implications for residual titanite in arc magma sources. *Journal of Geophysical Research* **94**, 4619–4633.

Remesal, M. B. (1988). Geología y petrología de los basaltos de la Meseta de Somuncurá. Ph.D. dissertation. University of Buenos Aires, 207 pp.

Remesal, M. B. & Parica, C. A. (1989). Caracterización geoquímica e isotópica de basaltos del sector noreste de la Meseta de Somuncurá. *Revista de la Asociación Geológica Argentina* **44**, 353–363.

Remesal, M. B., Méndez, M. J. & Gagliardo, M. (2002). Petrología de la secuencia volcánica cenozoica en el área del arroyo Ranquil Huao: Meseta de Somún Curá, Patagonia Extraandina. *Revista de la Asociación Geológica Argentina* **57**, 260–270.

Rhodes, J. M. (1996). Geochemical stratigraphy of lava flows sampled by the Hawaii Scientific Drilling Project. *Journal of Geophysical Research* **101**, 11729–11746.

Rudnick, R. L. & Fountain, D. M. (1995). Nature and composition of the continental crust—a lower crustal perspective. *Reviews in Geophysics* **33**, 267–309.

Scarrow, J. H. & Cox, K. G. (1995). Basalts generated by decompressive adiabatic melting of a mantle plume: a case study from the Isle of Skye, NW Scotland. *Journal of Petrology* **36**, 3–22.

Silver, P. G., Russo, R. M. & Lithgow-Bertelloni, C. (1998). Coupling of South American and African plate motion and plate deformation. *Science* **279**, 60–63.

Sleep, N. H. (1990). Mantle composition and processes. In: Saunders, A. D. & Norry, M. J. (eds) *Magmatism in the Ocean Basins. Geological Society, London, Special Publications* **42**, 313–345.

Somoza, R. (1998). Updated Nazca (Farallón)–South America relative motions during the last 49 m.y.; implications for mountain building in the Central Andean region. *Journal of South American Earth Sciences* **11**, 3211–3215.

Spera, F. J. & Bohrson, W. A. (2001). Energy-constrained open-system magma processes I: general model and energy-constrained assimilation–fractional crystallization (EC-AFC) formulation. *Journal of Petrology* **42**, 999–1018.

Stern, C. R. (1991). Role of subduction erosion in the generation of Andean magmas. *Geology* **19**, 78–81.

Stern, C. R., Frey, F. A., Futa, K., Zartman, R. E., Peng, Z. & Kyser, T. K. (1990). Trace element and Sr, Nd, Pb, and O isotopic composition of Pliocene and Quaternary alkali basalts of the Patagonian plateau lavas of southernmost South America. *Contributions to Mineralogy and Petrology* **104**, 294–308.

Sun, S.-s & McDonough, W. F. (1989). Chemical and isotopic systematics of oceanic basalts; implications for mantle composition and processes. In: Saunders, A. D. & Norry, M. J. (eds) *Magmatism in the Ocean Basins. Geological Society, London, Special Publications* **42**, 313–345.

Tolan, T. L., Reidel, S. P., Beeson, M. H., Anderson, J. L., Fecht, K. R. & Swanson, D.A. (1989). Revisions to the estimates of the areal extent and volume of the Columbia River basalt group. In: Reidel, S. P. & Hooper, P. R. (eds) *Volcanism and Tectonism in the Columbia River Flood-basalt Province. Geological Society of America, Special Papers* **239**, 1–20.

Turcotte, D. L. (1995). How does Venus lose heat? *Journal of Geophysical Research* **100**, 16931–16940.

Turner, S. & Hawkesworth, C. (1995). The nature of the subcontinental mantle: constraints from the major element composition of continental flood basalts. *Chemical Geology* **120**, 295–314.

Watson, S. (1993). Rare earth element inversions and percolation models for Hawaii. *Journal of Petrology* **35**, 763–783.

White, W. M. & Duncan, R. A. (1996). Geochemistry and geochronology of the Society Islands: new evidence for deep mantle recycling. In: Basu, A. & Hart, S. (eds) *Earth Processes: Reading the Isotopic Code. Geophysical Monograph, American Geophysical Union* **95**, 183–206.

Wilson, M. & Guiraud, R. (1992). Magmatism and rifting in western and central Africa from Late Jurassic to Recent times. *Tectonophysics* **213**, 203–255.

Yang, H.-J., Frey, F. A., Rhodes, J. M. & Tatsumoto, M. (1996). Evolution of the Mauna Kea volcano: inferences from lava compositions recovered in the Hawaii scientific drilling project. *Journal of Geophysical Research* **101**, 11747–11747.

APPENDIX

Table A1: *Somuncura province volcanic sample locations*

Sample:	Lat. (S)	Long. (W)	Topographic sheet*	Locality description
Pre-plateau and plateau volcanic rocks				
CH1	42°38′	68°10′	Gan Gan	Sierra de Chacays on Route 11, ~20 km south of Chacays Oeste school
CH2A	42°38′	68°04′	Gan Gan	Sierra de Chacays on Route 11, 4 km south of CH1
RHA1& 2	42°36′	67°12′	Telsen	Ranquil Hauo, basal flow
RHB to RHG	42°36′	67°12′	Telsen	Ranquil Huao, section east of puesto, B is basal flow, G is top
RH6 to RH1	42°36′	67°12′	Telsen	Ranquil Huao, continue sequence above RHG west of puesto, RH1 is top flow
TM2 & Ad200	42°27′	67°02′	Telsen	Basal flow below Ad 209, south of Route 4, west of village of Telsen
T1	42°25′	66°49′	Telsen	NE of Telsen on road to Coña Niyeu, ~2 km south of Estancia Blanca
T3	42°26′	66°46′	Telsen	NE of Telsen on road to Coña Niyeu, south of Estancia Blanca
GG1	42°22′	67°31′	Gan Gan	South side Route 4, west of Telsen, west of Puesto Abdal
GG6	42°29′	67°56′	Gan Gan	South of Bajo Hondo, Route 4 between Telsen and Gan Gan, Sierra de Apas
GG8	42°31′	68°01′	Gan Gan	West of GG7 along Route 4 between Telsen and Gan Gan
GG7D	42°31′	67°59′	Gan Gan	West of GG7 along Route 4 between Telsen and Gan Gan
GG9F to GG9B	42°26′	68°17′	Gan Gan	Sequence north of Gan Gan on road to El Caín, B is top
M10	41°42′	68°02′	Maquinchao	East of El Caín on road to Gan Gan near Ea La Querencia, below M11
M1	41°31′	68°36′	Maquinchao	Eroded flow on east side Route 5, ~30 km south of town of Maquinchao
CH4A	42°53′	67°28′	Telsen	Bajada del Diablo, north side of road
CN1	41°45′	66°33′	Coña Niyeu	East of Coña Niyeu, north side of road to town of Sierra Grande
CN2A	41°43′	66°18′	Coña Niyeu	East of Coña Niyeu, north side of road to town of Sierra Grande
CN3	41°43′	66°18′	Coña Niyeu	East of Coña Niyeu, north side of road to town of Sierra Grande
CN3-2	41°43′	66°18′	Coña Niyeu	East of Coña Niyeu, north side of road to town of Sierra Grande
CN4AA to CN4F	41°41′	67°06′	Coña Niyeu	Rincón Grande, north of Estancia San Nicholas, AA and A is top, F is base
B26	40°50′	65°55′	4166-1	Near Aguada Cecilio along Route 23
Val1	40°50′	65°55′	4166-1	Near B26, ~30 km east of Valcheta along Route 23 at Aguada Cecilio
B19	41°07′	65°56′	Coña Niyeu	Basalto Pailemán, south of Aguada Cecilia, east of El Tembrao
BC2	40°39′	66°46′	4166-1	Near Puesto Corayan, flow remnant near Chipauquil police station
Val3-1 to 3-5	40°54′	66°38′	4166-1	Section south of Valcheta, west of Estancia El Rincón, 3-1 is base
Val2B to Val2C	40°59′	66°39′	4166-1	Basal flow sequence west of Val3; west of Chipauquil, west of Estancia El Rincón
BSC11	40°28′	66°52′	4166-1	Puesto Alberto Rodriguez near La Angostura, Route 23
Ang1A & 1B	40°30′	66°55′	4166-1	Flows at La Angostura along Route 23 near BSC11
B14	40°35′	66°54′	4166-1	Cerro Cabeza de Vaca, south of La Angostura
B31	40°30′	67°13′	4166-1	Cerro Tapileigue near Ramos Mexía, Route 23
Som4	41°04′	68°32′	Maquinchao	NE of Cerro Traquén Negro, Route 23, lower flow
Mac1	41°04′	68°26′	Maquinchao	Meseta de Coli Toro flow, Route 23, SE of Aguada de Guerra
Mac2	41°09′	68°25′	Maquinchao	Meseta de Coli Toro flow, ~20 km east of town of Maquinchao

Table A1: continued

Sample:	Lat. (S)	Long. (W)	Topographic sheet*	Locality description
Mac3A to 3C	41°17′	68°57′	Maquinchao	Epu Lafquen flow sequence, south of Route 23, 19 km west of town of Maquinchao, A is top flow
Pat12A &12B	41°17′	68°54′	Maquinchao	Epu Lafquen flow sequence, south side Route 23, west of town of Maquinchao
Pat11A to C	41°38′	69°13′	Ing. Jacobacci	Meseta Cari-Laufquen, Quebrada Abi Saad, north of town of Ingenierio Jacobacci, A is top flow
Pat15A to C	41°03′	70°13′	Ing. Jacobacci	Sequence along Route 23, ~5 km east of Comallo, A is top flow, C is base
CP1	41°02·5′	70°15′	Ing. Jacobacci	Flows just north of village of Comallo
CP2	41°02·5′	70°15′	Ing. Jacobacci	Flows just north of village of Comallo
Post-plateau volcanic rocks				
CH4B to CH4D	42°53′	67°28′	Telsen	Bajada del Diablo sequence along road to north, D is basal flow
CH5A	42°52′	67°26′	Telsen	Bajada del Diablo, road to north just east of CH4, massive flow
Ad101a	41°57′	67°34′	Gan Gan	Sierra de Apas; Cerro Marasella
TM1	42°28′	67°00′	Telsen	Basalto La Meseta, south of Route 4, west of village of Telsen, top flow
Ad209	42°28′	67°00′	Gan Gan	Basalto La Meseta, south of Route 4, west of village of Telsen, upper flow
Ad46	42°15′	67°39′	Gan Gan	Bajo Hondo Basalt
Ad48	42°14′	67°47′	Gan Gan	Bajo Hondo Basalt
Ad58	42°15′	67°55′	Gan Gan	Bajo Hondo Basalt
Ad68	42°17′	67°58′	Gan Gan	Bajo Hondo Basalt, Cola de Occidental
GG7A to GG7D	42°31′	67°59′	Gan Gan	South side of Route 4, Cañadón Pelado sequence, D is basal flow
Ad304	42°35′	67°49′	Gan Gan	Sierra de los Chacays, south of Evans Jose
GG9A	42°26′	68°18′	Gan Gan	Base of GG9B to GGF sequence
M11	41°41′	68°02′	Maquinchao	East of El Caín on route to Gan Gan near Estancia La Querencia, above M10
Ad307	42°56′	67°56′	Gan Gan	Mirasol Chica, Sierra La Colonia, Puesto Sartre
M2A to M2C	41°29′	68°36′	Maquinchao	Sequence east of Estancia El Triangular, north side of Route 5, ~35 km south of Maquinchao, A is top flow
M3	41°30′	68°33′	Maquinchao	Flow on Cerro Mirador, south side of Route 5 midway Maquinchao and El Caín
M4	41°30′	68°32′	Maquinchao	Flow 3 km east of M2 sequence along Route 5 between Maquinchao and El Caín
M5	41°34′	68°24′	Maquinchao	Flow at Cerro Mirador south of Route 5 between Maquinchao and El Caín
M6	41°37′	68°21′	Maquinchao	Flow 21 km east of M3 along road, west of El Caín
Val2A	40°59′	66°35′	4166-1	Top of flow sequence at Chipauquil, north of Valcheta
Silicic volcanic rocks (Quiñelaf I and II Formations)				
GG5	42°21′	67°42′	Gan Gan	North side of Route 4, Cerro El Gaucho, mica-bearing, porphyritic benmoreite neck
GG3	42°22′	67°39′	Gan Gan	Cerro Las Hueyas, south of Route 4 between GG2 and GG5, benmoreite flow
GG4	42°24′	67°34′	Gan Gan	South of Route 4, NE of Puesto Aguada de la Noche, ignimbrite–pyroclastic flow
M12 & M13	42°05′	68°14′	Maquinchao	Pampa de Talagapa, north of town of Gan Gan, pyroclastic flows east of road near km 877
GG2	42°37·5′	67°35′	Gan Gan	North of Route 4, east of town of Telsen, Cerro Cayuqueo, dome?

*Latitude and longitude from 1:250 000 topographic sheet indicated.

Table A2: Parameters used in EC-AFC models in Fig. 11

Type:	Hawaiian tholeiite	Plan-Luan xenolith	Lower crust	Upper crust	Chon Aike rhyolite
Role:	mafic magma	assimilant	assimilant	assimilant	assimilant
Trace elements and distribution coefficients used					
Sample or source	R117	Chacays2	standard	standard	453
Sr (ppm)	275	682	348	350	318
high D_{Sr}	1·5	1·5	1·5	1·5	1·5
low D_{Sr}		0·05	0·05		
Nd (ppm)	13·1	4·8	11	26	37·3
D_{Nd}	0·25	0·25	0·25	0·25	0·25
Th (ppm)	0·5	assume 1·1	1·2	10·7	12·3
D_{Th}	0·1	0·1	0·1	0·1	0·1
Isotopic ratios used—adjusted to 27 Ma					
$^{87}Sr/^{86}Sr$	CH1 or RHA2	0·706689	0·710000	0·722000	0·710470
$^{143}Nd/^{144}Nd$	CH1 or RHA2	0·512368	0·512200	0·511800	0·512130
εNd	CH1 or RHA2	−5·3	−8·5	−16·3	−9·9
Temperatures (°C) used with assimilant					
Magma liquidus		1320	1320	1280	1280
Magma initial		1320	1320	1280	1280
Assimilant liquidus		1100	1100	1000	1000
Assimilant initial		600	600	300	300
Solidus		950	950	900	900
Equilibration		980	980	980	980

D, magma distribution coefficient for element indicated. Lower and upper crustal concentration data are from Rudnick & Fountain (1995); Chon Aike trace element data from sample 453 in Table 6; Chon Aike isotopic data and Plan-Luan lower crustal xenolith (sample Chacays2) trace element and isotopic ratios from Pankhurst & Rapela (1995); Hawaiian trace element data from Yang *et al*. (1996); and Somuncura pre-plateau lava CH1 and RHA2 isotopic data from Table 7. Temperatures are those used in models of the Columbia River basalts and other localities by Bohrson & Spera (2001).